J Mater Sci (2016) 51:640–667
DOI 10.1007/s10853-015-9440-z

REVIEW

CVD growth of 1D and 2D sp^2 carbon nanomaterials

Jinbo Pang[1] · Alicja Bachmatiuk[1,2] · Imad Ibrahim[1,3] · Lei Fu[4] · Daniela Placha[5] · Grazyna Simha Martynkova[5] · Barbara Trzebicka[2] · Thomas Gemming[1] · Juergen Eckert[1,3,6] · Mark H. Rümmeli[1,2,5]

Received: 11 August 2015 / Accepted: 14 September 2015 / Published online: 21 September 2015
© Springer Science+Business Media New York 2015

Abstract The discovery of graphene and carbon nanotubes (rolled-up graphene) has excited the world because their extraordinary properties promise tremendous developments in many areas. Like any materials with application potential, it needs to be fabricated in an economically viable manner and at the same time provides the necessary quality for relevant applications. Graphene and carbon nanotubes are no exception to this. In both cases, chemical vapor deposition (CVD) has emerged as the dominant synthesis route since it is already a well-established process both in industry and laboratories. In this work, we review the CVD fabrication of graphene and carbon nanotubes. Initially, we briefly introduce the materials and the CVD process. We then discuss pretreatment steps prior to the CVD reaction. The discussion then switches to the CVD process, provides comparative data for thermal CVD and plasma-enhanced CVD, and includes coverage of kinetics, thermodynamics, catalyst choice, and other aspects of growth as well as post production treatments. Finally, conclusions are drawn and presented.

✉ Mark H. Rümmeli
m.ruemmeli@ifw-dresden.de

[1] IFW Dresden, PO Box 270116, 01171 Dresden, Germany

[2] Centre of Polymer and Carbon Materials, Polish Academy of Sciences, M. Curie-Sklodowskiej 34, 41-819 Zabrze, Poland

[3] Center for Advancing Electronics Dresden, TU Dresden, 01062 Dresden, Germany

[4] College of Chemistry and Molecular Science, Wuhan University, Wuhan 430072, China

[5] Nanotechnology Centre, VSB-Technical University of Ostrava, 17. listopadu 15, 708 33 Ostrava-Poruba, Czech Republic

[6] Technische Universität Dresden, Institute of Materials Science, 01062 Dresden, Germany

Introduction

Carbon allotropes

Carbon materials consist of various allotropes. Carbon allotropes form when carbon atoms form covalent bonds between each other. There are several known carbon allotropes such as diamond, graphite and amorphous carbon. These are the traditional 3D bulk carbon materials. More recently, with the advent of advanced observation techniques, 2D graphene and 1D carbon nanotubes (CNTs) are identified as other, low-dimensional sp^2 carbon allotropes.

To understand sp^2 carbon, one can start with the electron orbital hybridization [1, 2]. Carbon's atomic number is six. It has four valence electrons which occupy the $1s^2$, $2s^2$, $2p_x^1$, and $2p_y^1$ atomic orbitals. With all four of the valence electrons contributing to covalent bonds, carbon is tetravalent and forms sp^3 carbon, which we more commonly know as diamond. The bonding energy between two sp^3 carbon atoms is 3.6 eV and contributes to diamonds' great strength. Carbon can also form with sp^2 hybridization in which three electrons form in-plane σ (covalent) bonds and the fourth electron forms a weak (non-covalent) inter-plane π bond. The π electrons are delocalized and provide graphite (and graphene) with its electrical conductivity. The inter-plane π bond has relatively low bonding energy of 31 meV [3] in comparison to the very strong in-plane σ bond (6.4 eV). This means that graphite is a layered structure formed from graphene layers that can easily slide apart from each other and it is this easy sliding action that

allows us to use graphite for graphical purposes (e.g., a graphite pencil) and from which it derives its name.

Indeed, the individual graphite layers can be separated and ultimately yield a single layer, which we term graphene [1, 4]. The three equivalent sp^2 σ orbitals are symmetrically angled with 120° in the *X*–*Y* plane (forming a characteristic hexagonal or honeycomb lattice), while non-hybrid 2p-orbitals are perpendicular to the *X*–*Y* plane. One can also take sections of a graphene sheet that can then be rolled up into a ball which we call a fullerene. In this case, some pentagon structures form amid the hexagons to allow for curvature much like a classic leather football. One can also roll up a graphene sheet to form a tube, and we call these structures single-walled carbon nanotubes. When several sheets are rolled up, we obtain multi-walled carbon nanotubes.

Graphene and carbon nanotubes

The properties vary between the various carbon allotropes, and thus each is of interest for a variety of applications. Indeed, so rich are their applications it would be too much to enter into in this review. Here, we focus only on the chemical vapor deposition (CVD) for the fabrication of graphene and CNTs since this growth route is the most promising for their manufacture in the semiconducting industry when considering both CNTs and graphene as important future materials in the electronics industry as well as for mass production. At first, we briefly look at the properties of graphene and CNTs that make them so promising and then we introduce the reader to CVD as a growth route.

Type and properties of graphene

In terms of morphology, graphene can be classified into planar graphene and vertical graphene. Planar graphene lies parallel to a substrate. With increasing layer numbers, planar graphene is usually divided into three types, namely mono-, bi-, and multi-layer graphene. In contrast, vertical graphene is free standing and anchor perpendicular to a substrate.

The enormous interest in graphene has been mostly driven by its unique electronic and electrical properties. Monolayer graphene has three key electronic properties. These have zero carrier density at the Dirac points and are pseudo-spin and relativistic carriers [1, 4]. These electronic properties provide a rich series of experiments in physics, such as modulation of carrier density with tuning gate voltage, quantum hall effect [5, 6], and band gap engineering in graphene ribbons [7, 8]. Thus, graphenes are potentially building blocks for transistors [9]. Bilayer graphene [10], especially with AB-Bernal stacking [11–13], has tunable band gap depending on the gate voltage [14, 15]. Few-layer graphene is better suited for application in electrochemical energy systems [16–20] as opposed to device use. Vertical (multi-layer) graphene [21–23] has a curved and folded morphology in contrast planar graphene. Multi-layer graphene (graphite) is generally used as a catalyst support and as electrodes in energy systems [24–32].

With the strong C–C bond in sp^2 carbon, graphene yields the highest intrinsic strength of known materials [33, 34]. The graphene nano-platelets can blend with polymer for a composite [35] with reinforced mechanical strength and electrical conductivity. The thermal conductivity of graphene is also very high ($\sim$2000 W mK^{-1}) and is the highest among all the carbon allotropes [1]. The optical conductance of graphene is independent of frequency over a wide range [36, 37].

An ideal graphene sheet comprises a perfect hexagon network similar to honeycomb. However, the pentagon and heptagon pairs are commonly observed in non-perfect graphene. The typical locations where such pairs are observed are in grain boundaries [38, 39], folded edges [40], and electron-irradiation-induced defects [41, 42]. The pentagon and heptagon pairs degrade the electronic conductance of graphene by introducing electron scattering sites [43, 44]. Moreover pentagon–heptagon pairs will also deform the graphene [45, 46]. Hence the production of single-crystal graphene via CVD approach is highly attractive to avoid the drawbacks of defects.

Moreover, the chemical properties of graphene can be modified by introducing functional groups [47–52]. The chemical functionalization can disrupt pristine graphene with covalent bonds or van der Waals interactions of external groups or molecules [53, 54]. The intercalation of molecules between two graphene sheets is a means with which to obtain graphene and few-layer flakes. The large surface area of graphene-based complex materials (with functional particles) is also attractive in applications such as biological sensors [55], humidity sensors [56], antibacterial devices [57], complex anode material for Li-ion batteries [58], and catalyzed H_2 generation [59].

Type and properties of CNTs

CNTs are fundamentally distinct as compared to graphene as they have curvature, viz. planar graphene has zero curvature, while carbon nanotube has a diameter (chirality)-dependent curvature [60]. The curvature influences the physical properties of CNTs such as electrical [61–63], vibrational [64, 65], optical [66, 67], thermal [68, 69], and mechanical properties [70]. For ideal planar graphene, the electrical properties are dominated by the delocalized electrons in π orbital. For single-wall carbon nanotubes, the

electrical properties differ because of the re-hybridization of π–σ orbitals due to the curvature effect [71–74]. When tube diameter is small (<2 nm), the chirality plays a role in the curvature effect and thus the physical properties [75].

In comparison to graphene, CNTs can be classified by wall numbers into three categories. They are single-walled nanotubes (SWNTs), double-walled nanotubes (DWNTs), and multi-walled nanotubes (MWNTs). SWNTs can be further divided into metallic, semi-metallic, and semiconducting according to their chiral angle. DWNTs have two layers of walls which is convenient for further functionalization [2, 76, 77] while preserving the straightness of the tube (since in the SWNT case the tube wall can collapse upon the introduction of defects/functionalization). MWNTs have various morphologies in which, for example, they can have parallel walls (concentric tubes within each other) [78–80], a bamboo-like structure [81, 82], or a herringbone structure [83].

The large scientific and industrial interests in CNTs have been driven by the amazing electronic properties [84]. Depending on their electronic properties, SWNTs can be divided into metallic and semiconducting types [2]. Firstly, the metallic CNTs show ballistic transport behavior, i.e., electrons pass along the tube with little or no scattering. In other words, almost no heat is dissipated inside it, viz. CNT is capable of conducting large current while avoiding an excessive temperature increase. This conductivity behavior is attractive in integrated circuits in that transparent electrodes can be formed with metallic CNT networks [85]. Semiconducting SWNTs transport electrons in a diffusive manner. However, experiments show a high mobility in semiconducting SWNTs. Indeed, the electronic property of SWCNTs depends on their diameters and helicity [86]. This leads to exciting application potential in devices such as diodes, field-effect transistors [87, 88], field emitters, and memories [89]. CNTs can also be mixed into composite materials for energy applications such as electrodes for fuel cells [90], lithium/sodium ion batteries [91, 92], and super capacitors [93, 94] and used as a catalyst for photo-electricity transformation [95, 96] and as a supporting matrix [97].

As previously mentioned, the electrical properties of SWNTs are strongly related to their chirality. One can image SWCNT as a rolled-up graphene nanoribbon. Thus, the SWNT structure can be indexed with an integer pair (n, m), which serves as a rolling vector [98–102]. When n is equal to m, the SWNTs have an armchair tube opening. They are metallic CNTs (no band gap) [103, 104]. Armchair SWNTs remain metallic regardless of tube diameter. When $(n-m)/3$ is a non-zero integral, the tube edges are zigzag. They are semi-metals with a small bandgap [99, 105, 106]. Each of their bandgaps is proportional to the inverse of the diameter squared [99, 107–109]. When $(n-m)/3$ is any other value (non-integer), the SWNTs have a chiral angle, depending on (n, m). Each of these semiconducting SWNTs has a bandgap that is proportional to the inverse of the tube diameter [110–112]. The representative values of the band gap are listed in Table 1.

Perfect CNTs have hexagon lattice structure. However, like graphene, the introduction of pentagon and heptagon pairs will alter the tube helicity and therefore its electronic structure [99, 117–122]. One advantage of the introduction of a pentagon and heptagon pair is the creation of on-tube tuning of tube chirality/helicity. For example, a semiconducting/metallic junction (8, 0)/(7, 1) can form when introducing pentagon–heptagon pairs along the (8, 0) axial direction [122]. A semiconducting heterojunction (10, 0)/(9, 1) can form when inserting a pentagon–heptagon pair on a (10, 0) tube axis [122]. A complicated configuration of pentagon and heptagon pairs can build up a metal–metal junction such as (12, 0)/(6, 6) and (9, 0)/(6, 3) as well [123].

Another attractive property of CNTs is their mechanical properties [124, 125]. The tensile strength of the stiffest CNTs is approximately fifty times larger than that of steel, while their Young's modulus is five times larger than that of steel. CNT can tolerate 30 % induced strain so that structural enhancement can be achieved when using CNT in polymer composites [124, 126–129], metal powders [130], and ceramic matrices [131]. Besides, functionalization of MWNT with silane molecules enables the better solubility (chemical compatibility) for polymer matrix composites [132]. Also, CNT can be used as robust microscope probes [133] and nanoscale tweezers [134]. The thermal conductivity of MWNTs (from arc-evaporation production) exceeds 3000 W mK^{-1} [135]; however, MWNTs from catalytic CVD methods show a significant drop in thermal conductivity down to 200 W mK^{-1} [136]. Probably, the presence of catalysts impurities (usually metal particles) degrades the thermal conductivity by creating scattering sites.

The chemistry of CNT is more rich than that of graphene since it has a different chemistry on its inside and outside. This is one advantage of CNT over graphene, in which both sides are symmetric and show no difference. Moreover, one can take the advantage of the nanoscale space inside a SWCNT [137]. The filling of heterogeneous substances into CNTs can also be achieved [138–140]. Some fillings hold potential in magnetic material engineering [80, 141]. The inside of a CNT can also be used to adsorb gas molecules, such as hydrogen [142–145], nitrogen monoxide [146], nitrogen, and oxygen [147] as well as Xe [148]. The tube interior can work as a nano-channel of fluidics to let water [149] or solutions flow [150] through. The filling of CNT with water can work as a valve to switch on/off the transport of gas molecules [151] and a

Table 1 The relation between the type, the bandgap, and SWNT index is listed. The small band gap dependent on the diameter shows a curvature effect for semi-metallic and semiconducting SWNTs, viz. the band gap increases with decreasing tube diameter

Type (metallic, semi-metallic, semiconducting)	Diameter (nm)	Bandgap (eV)	SWNT index (n, m)	Ref.
Metallic	0.81	0	(6, 6)	[103]
Metallic	1.08	0	(8, 8)	[103]
Metallic	1.21	0	(9, 9)	[104]
Semi-metallic	0.47	0.21, 0.05	(6, 0)	[73, 107]
Semi-metallic	0.70	0.08	(9, 0)	[105]
Semi-metallic	0.93	0.04	(12, 0)	[105]
Semi-metallic	1.17	0.03	(15, 0)	[105]
Semiconducting	0.43	2.02	(4, 2)	[113]
Semiconducting	0.48	1.77	(4, 3)	[114]
Semiconducting	0.70	1.42	(6, 4)	[114, 115]
Semiconducting	0.74	1.27	(6, 5)	[116]
Semiconducting	0.81	1.21	(7, 5)	[116]
Semiconducting	0.96	1.00	(9, 5)	[116]
Semiconducting	1.01	0.98	(8, 7)	[116]

hydroelectric power generator [152]. With water filling, the phase transformation can be observed inside the tube, for example, ordered water [153] and ice crystals [154]. CNT with encapsulated catalyst particles can function as a nanoreactor for ethanol production [155], Pd-catalyzed hydrogenation [156], Pt-catalyzed fuel cell [157], and inner smaller CNT growth [158]. The encapsulated catalysts exhibit a confinement effect [159] from the tube diameter. The confinement effect can enhance the capacitance of encapsulated MnO_2 [160] and the electron spin of encapsulated transition metals [161] such as Gd [162]. The filling of DNA molecule inside a tube enables biological application [163]. Moreover, a single-molecule biological activity (with retinal molecule inside a carbon nanotube) can be imaged dynamically in response to light exposure [164].

The outside of a CNT has the merit of a large surface-to-volume ratio, which provides a reactive surface. The chemistry of CNT exteriors can be tuned with covalent or non-covalent functionalization. Covalent functionalization aims to solubilize the CNTs by attaching hydrophilic species to them [165]. This aggressive process though can disrupt the structure of the tube walls. In contrast, non-covalent functionalization binds molecules gently to CNTs via Van der Waals forces without degrading the tube [166–168]. When the biological molecules such as protein and DNA are used, biological functionalization can be obtained [169]. Functionalization of carbon nanotube can work as a drug delivery platform [170]. As above, the functionalization occurs at/over the wall structure. One can also dope CNT by replacing C in the wall with other elements such as B and N [171–173], and BN nanotube was individually synthesized when C is totally replaced by both B and N [174–176].

Chemical vapor deposition

CVD is a sophisticated synthesis technique for both industry production and laboratory research. CVD is applied in many areas, such as crystal growth, thin-film coating, and fiber and powder production. CVD is also well developed for the synthesis of graphene and carbon nanotubes. The principles of CVD [4] for sp^2 carbon include two steps, firstly thermal decomposition of carbon feedstock and thereafter re-assembly of carbon radicals into sp^2 carbon nanostructures.

The carbon feedstock varies according to the hydrocarbon selected. Examples include gaseous methane, ethylene, and acetylene, as well as solvents such as methanol, ethanol, isopropanol, and acetone and aromatic hydrocarbons. Usually, catalytic metals are used during CVD to enhance decomposition of the feedstock and perhaps also to aid sp^2 carbon assembly.

Catalyst choices are often transition metals, for example, Fe, Co, and Ni for CNT growth and Cu and Ni for graphene CVD growth. However, the non-catalytic substrates are emerging for sp^2 carbon growth and also, for example, Si/SiO_2 wafers.

In terms of the heating source, there are two types of CVD, conventional thermal CVD and plasma-enhanced CVD. In a thermal CVD system, the heat generated from a resistance heating element is transferred to the target substrate and feedstock gas.

In a plasma-enhanced CVD oven, a plasma source is added to assist the thermal cracking of the carbon feedstock. Plasma CVD has certain benefits, such as that it decreases the growth temperature and thus, for example, minimizes catalyst particle agglomeration which is important for CNT growth. However, in terms of synthetic graphene by plasma CVD it is very desirable for growing vertical graphene but has limited potential for nano-crystalline planar graphene (thus far).

In terms of gas pressure during CVD synthesis, one can work at atmospheric pressure or at low pressure. Generally, low-pressure CVD facilitates rapid growth due to the larger probability of carbon species at the substrate. In contrast, ambient-pressure CVD is economic as it avoids the need for a complicated vacuum system but has lower growth kinetics.

CVD growth of graphene

There are many routes with which to fabricate graphene. These include mechanical exfoliation [177], reduced graphene oxide [178–180], (electro-) chemical exfoliation [181, 182], ribbon formation by unzipping CNTs [183, 184], bottom-up synthesis from aromatic molecular precursors [185], epitaxial growth over silicon carbide [186, 187], segregation upon transition metals on cooling [188–191], organic molecule adsorption with post hydrogen annealing [192], e-beam irradiation-driven graphene growth [193], and CVD [16, 23, 194–196]. When synthesizing graphene for electronic devices, graphene is generally required to form over a large area. Moreover, graphene should ideally be crystalline with negligible defects. Balancing the production cost and the above prerequisites, CVD is the most promising route to produce large-area device-grade graphene. Indeed, graphene synthesis by CVD is one of the most popular techniques because of its potential to be scaled up, and it is already well established both in industry and in research labs.

Substrate pretreatment

Prior to graphene synthesis by CVD, substrate preparation is important. Substrates for graphene growth can be classified into two categories. They are metals and non-metals. When using metals such as Cu, the pretreatments before CVD include general surface cleaning via organic solvent soaking [197], partial Cu surface etching with strong HNO_3 [198] or weak acetic acid [199], smoothing the surface with electrical or chemical mechanical polishing [200, 201], passivating the surface with oxygen [199] or argon exposure [202], surface rearrangement and grain size increase with H_2 annealing [4], liquefied Cu above its melting point [203, 204], and thorough removal of carbon contamination by air sintering [195, 205].

Without any pretreatment, second-layer flakes form probably beneath a full coverage of monolayer graphene from trapped carbon species [206]. With pretreatments [200, 201, 207], carbon diffusion is suppressed because there is a lack of carbon-trapping sites (e.g., Cu grooves and contamination from the supplier processing).

Oxygen, in particular, plays an important role in fabricating both single-crystal graphene [199, 202] and large-area strict monolayer graphene film [195, 205]. Oxidation treatment is vital to remove surface organic contaminant, as shown in Fig. 1.

In terms of Ni supports, the optimization of the thickness of Ni film upon a support (e.g., Mo foil or Si/SiO_2 wafer) is crucial to control the number of graphene layers and the homogeneity of the graphene layers by controlling the C solubility which is high in Ni [188, 190, 208].

When employing non-metal substrates, for example, silicon oxide or silicon nitride, usually cleaning in organic solvents is used initially [209]. Oxygen treatment (air burning 800 °C for 1 h) [210] is also implemented, and this has been shown to enhance the nucleation of graphene.

Thermal chemical vapor deposition

Thermal CVD typically results in planar graphene with controlled layer numbers such as mono-, bi-, and multilayer graphene. In a thermal CVD procedure, Ni and Cu are the most popular substrates to grow graphene [4] though a few works use Ru [211], Co [212], Fe [213, 214], and Ag [215]. Polycrystalline Ni films (on Si/SiO_2 support) facilitate the formation of thin continuous graphene films (layer number varies from 1 to 10) at ambient pressure [216, 217] and also at low pressure [218]. Single-crystal Ni (111) is good for the efficient growth of monolayer graphene (coverage ca. 90 %), while Ni polycrystalline foil has a lower yield (72 %) [4]. Among all the substrates, Cu currently attracts the most attention because it is far easier to grow monolayer graphene due to the low carbon solubility found in Cu. In general, the polycrystalline graphene grain sizes found with Cu are larger than those found in Ni [4]. In polycrystalline Cu, monolayer graphene is usually argued to grow in a self-limited manner [194]. A further advantage of Cu as a substrate is that it can be scaled up relatively easily for large-area graphene fabrication such that even 30-inch graphene transparent films transferred in a roll-to-roll approach have been demonstrated [219]. In an effort to remove the need to etch copper away from synthetic graphene after synthesis, the use of thin Cu films over Si/SiO_2 [220] can be advised as it sublimes during the reaction such that at the end only graphene remains [221].

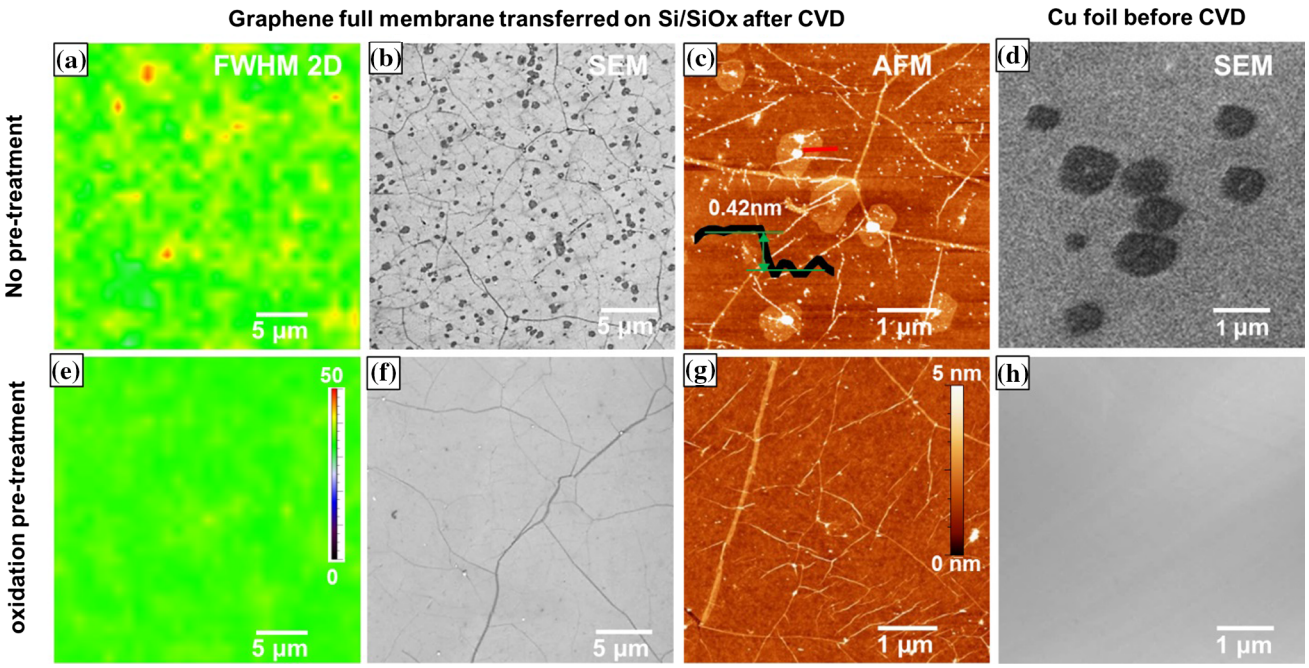

Fig. 1 Influence of oxidation pretreatment on the graphene formation over Cu foil. CVD-grown graphene without pretreatment: **a** Raman mapping of full width half maximum of 2D mode, **b** SEM images of graphene transferred on Si/SiO_x, and **c** AFM images of the same graphene. And graphene growth with oxidation pretreatment: **e** Raman mapping of FWHM 2D, **f** SEM images of graphene transferred on Si/SiO_x, and **g** AFM images of the graphene. The SEM images of Cu foil before CVD growth: **d** without pretreatment, graphene flakes form **h** with oxidation pretreatment, Cu surface remains clean without graphene flake formation. Reprinted (adapted) with permission from Ref [195]. Copyright (2015) American Chemical Society

Another approach to avoid transfer (which can damage and contaminate the graphene) is to directly synthesize graphene over a non-metal substrate with no metals present. Non-metallic substrates include quartz [222], sapphire [223], Si/SiO_2 [210], Si_3N_4 film [224], MgO crystals [225], and hexagonal BN [226–228]. This form of CVD growth is slower than when using metals; however, at times there are advantages, for example, the electron mobility of graphene grown over Si_3N_4 was shown to exceed that of transferred graphene grown over Cu [224].

Plasma chemical vapor deposition

Plasma CVD leads to the formation of vertical graphene and also planar graphene. With plasma-enhanced CVD, one can grow vertical graphene on various substrates including metals and non-metals [22, 23]. Moreover, PECVD can speed up the growth rate of planar graphene on non-metal supports by 15 min to achieve full coverage, [229] as compared to thermal CVD by at least 4 h [210]. In addition, PECVD can decrease the growth temperature significantly, for example, at 600 °C [230] one can generate high-quality graphene, while thermal CVD usually requires temperatures of 1100 °C or above [222].

Carbon feedstock

The carbon feedstock for graphene growth is typically a hydrocarbon. They can be categorized into gas, liquid, and solid. The most frequently applied is gaseous methane (CH_4) [194, 196, 231, 232] in Cu-based CVD. Also, ethylene (C_2H_4) [233] and acetylene (C_2H_2) [212, 225] have been used successfully for growing graphene. Liquid carbon source commonly seen in laboratory CVD growth of graphene includes alcohols [234–240] (for example methanol, ethanol, isopropanol), acetone [234], large hydrocarbons [241–243] (pentane, hexane), and aromatic hydrocarbons [235, 244–246]. Solid carbon sources have also been explored such as carbon doping into bulk metals [247, 248], amorphous carbon [249–251], self-assembly monolayer [252], camphor [253–256], DNA [257], insect protein [258], flower petal [259], PMMA [260–266], PS polymer [267], and waste plastics [268].

The carbon feedstock for carbon nanotube growth is similar to that for graphene. They are methane [269, 270], ethylene [271–275], acetylene [276–278], alcohol [80, 279–285], and aromatic hydrocarbons [286–288]. Carbon monoxide [289] has also been used to grow single-walled carbon nanotubes.

Growth mechanisms and dynamics

Thermodynamics describes the possibility of a reaction. It can be evaluated through the activation energy (Ea). The reaction process initializes when one satisfies certain conditions to overcome the reaction energy barrier (e.g., by increasing temperature, introducing a catalyst, etc.). Kinetics, however, describes the reaction rate. The kinetics can be evaluated using kinetic constants, for example, the growth rate of graphene (such as increase rate in size, density, or coverage of graphene flake over Cu substrates). The kinetic constants can be obtained from statistics of the experimental data. To obtain thermodynamic information such as activation energies, one can plot the so-called Arrhenius plot which is the logarithm of a kinetic constant against the reciprocal of temperature.

Thermodynamics and activation energy

Now, we turn to the parameters that affect the Ea such as gas pressure, type of feedstock, type of substrate, oxygen incorporation, plasma enhancement, and catalyst. The activation energies are in the range of 1.5–3.7 eV in low-pressure Cu–methane CVD [199, 290–292]. When increasing the pressure to ambient atmosphere, Ea increases by ca. 3 eV [292].

With respect to the influence of carbon feedstock choice, when using ethane (C_2H_4) as an alternative carbon feedstock in low-pressure CVD, activation energies are similar in the range from 2.4 to 3.1 eV [293, 294]. When using small-molecule solvents (ethanol, acetone, and isopropanol), Ea decreases to 1.4–1.6 eV [192]. When using large aromatic hydrocarbons ($C_{22}H_{14}$ and $C_{24}H_{12}$), the Ea drops to 1.46 and 1.87 eV, respectively [246].

In terms of substrate choice, when using Co and Ru substrates (under vacuum), the activation energies show no significant difference to that found for Cu (1.4–2.9 eV) [294, 295]. However, when switching to non-catalytic oxides, large increases in Ea occur such as 4.75 eV for SiO_2 [210] and 6.75 eV for Si_3N_4 [224]. This highlights the importance of a catalyst in decreasing the reaction energy barrier.

A tiny amount of oxygen adsorbed on a Cu surface can reduce the Ea [199]. Oxygen incorporated with H_2 in the reactions can lead to the formation of OH radicals which decrease the energy barrier. Compared to thermal CVD, plasma-enhanced CVD (PECVD) significantly reduces the Ea to 1.03 eV [296]. In addition, metal promoters such as Ni [290] reduce the Ea to 1.7 eV from 3.7 eV. Indeed, Ni foil [290] (in the upstream of target substrates) has been shown to enhance the decomposition of the carbon feedstock and thereafter accelerate graphene growth. We list the Ea values in Table 2 for an overview.

We now look at the growth kinetics of graphene. The kinetic constants can be accelerated by increasing reaction temperature, reactant concentrations, and catalyst activity. Firstly, an increase in CVD temperature can accelerate graphene growth. Indeed at temperatures below 1000 °C, full graphene coverage does not occur and pores remain in the film even after 150 min of CVD growth [291]. With temperatures in the range from 720 to 800 °C, graphene growth saturates to 50–80 % coverage [297]. However, at the elevated temperature of 1000 °C full coverage can be achieved within 10 min of CVD reaction time [291, 297]. Secondly, the growth kinetics can be enhanced by an increase in reactive carbon species. Reactive species concentrations increase either with an increase in the methane partial pressure [298] or an increase in reactive carbon species. The carbon species concentration can also be enlarged by an increase in temperature [299, 300]. The amount of carbon (larger than the equilibrium level for nucleation) is attributed only to the carbon source choice [291].

Thirdly, the catalytic activity of Cu and Ni can improve the growth kinetics. Indeed, CVD on Cu or Ni substrates typically requires < 1 h to achieve full coverage graphene growth [194, 196, 216, 218]. However, the CVD duration over a non-catalytic ceramic oxides requires several hours or days [210, 222, 224].

Furthermore, metal vapor is an efficient means to speed up the growth kinetics [196, 301]. Specifically, Cu vapor trapping facilitates graphene full coverage growth in 10 s [195, 196], whereas 15 min CVD growth times are required in a non-trapping setup with the same growth conditions [196]. Methane decomposition into reactive carbon species is probably enhanced by the trapped Cu vapor.

To better understand the thermodynamic and kinetic aspects of graphene growth, in situ characterization techniques are being developed, e.g., in situ SEM [302, 303], LEEM [304, 305], and XPS [306].

Reaction mechanisms over Cu

Cu is probably the most often used substrate since, because of its low carbon solubility, monolayer graphene with full coverage can easily be obtained with monolayer ratios exceeding 95 %, [194] and strictly (100 %) monolayer graphene [195, 309, 310]. A surface-mediated self-limited mechanism [194] is proposed such that once the Cu surface is fully covered, the catalytic process of Cu ceases and hence so does graphene growth. However, the surface-mediated mechanism cannot account for the secondary formation of graphene. For example, second-layer (additional) patches emerge in full coverage monolayer graphene film [195, 196, 309], and even agglomerate into

Table 2 Thermodynamic activation energy (Ea) is listed from different works in the literature. The growth conditions are also included

Support	Carbon source	Ea (eV)	Temperature (°C)	CVD type	Pressure	Ref.
Cu	CH_4	5.0	950–1080	Thermal	Ambient	[292]
Cu	CH_4	3.7	850–1000	Thermal	Low	[290]
Cu	CH_4	2.74	900–1050	Thermal	Ambient	[307]
Cu	CH_4	2.6	750–1000	Thermal	Low	[291]
Cu	CH_4	2.0	950–1080	Thermal	Low	[292]
Cu	CH_4	1.5, 1.76	835–1035	Thermal	Low	[199, 308]
Cu	CH_4	1.7	850–1000	Ni-promoted thermal	Low	[290]
Cu	CH_4	1.03	500–900	Plasma-enhanced	Low	[296]
Cu	CH_4	0.92	835–1035	Oxygen-assisted thermal	Low	[199]
Cu	C_2H_4	2.4–3.1	900–1050	Thermal	Low	[293]
Cu	C_3H_6O, C_3H_8O, C_2H_6O	1.4-1.6	800–1025	H_2 annealing	Low	[192]
Cu	$C_{22}H_{14}$, $C_{24}H_{12}$	1.46, 1.87	550–1000	Thermal	Vacuum	[246]
Co	C_2H_4	1.4, 2.9	340–360	Thermal stage	Vacuum	[294]
Ru	C film	2	470–800	Thermal stage	Vacuum	[295]
Si_3N_4	CH_4	6.75	1150–1190	Thermal	Ambient	[224]
SiO_2	CH_4	4.75	1050–1190	Thermal	Ambient	[210]

parallel lines [311] and achieve full coverage for bilayer graphene [310].

It is argued that part of the reason for this is carbon diffusion into/out of Cu grain boundaries. For one case, the outside of Cu pocket is found to grow bilayer graphene [310]. However, with a tungsten foil inside the Cu pocket, monolayer graphene was achieved with tungsten argued to suppress carbon diffusion from the inside to outside of the pocket [310]. In another case, pulsed methane doses [309] as opposed to a continuous flow were introduced to deplete carbon for graphene growth to avoid carbon accumulation at Cu grain boundaries (and thereafter C diffusion to form second-layer flakes) Adsorbed solvent on the Cu substrate can also account for the additional graphene flake formation [192].

Some researchers propose that the carbon can diffuse through an initial graphene layer, nucleate, and form second-layer flakes underneath full coverage monolayer film [312–314]. They discuss second-layer graphene growing above the full first layer of graphene [13, 315, 316]. In short, the origin of second-layer flakes is still not fully understood.

Liquid Cu substrates can play an important role in the growth of single-crystal monolayer graphene. Cu foils liquefy at elevated temperatures above its melting point (1080 °C). Monolayer single-crystal graphene (either round or hexagonal shaped) were fabricated over liquid Cu [203, 204, 317]. The grain boundary free Cu surface suppresses carbon diffusion into the Cu bulk and thereafter avoids the formation of second-layer flakes from carbon extrusion (from accumulated sites in the Cu bulk, e.g., grain boundaries). The advantage of liquid Cu also applies to other metals such as In [204] and Ga [318]. In contrast, solid Cu suffers from the evolution of polycrystalline graphene [319].

The geometry and quality of graphene flakes are probably dependent on Cu grain orientation (in solid Cu). Cu(101) and Cu (110) facilitate four-lobe graphene domain formation [320]. Moreover, graphene ribbon can be selectively grown on Cu twin-crystal striped surfaces like the (001) facet [321] by controlling the methane partial pressure, whereas Cu (111) facets produce higher quality monolayer graphene with a higher growth rate than Cu (100) facets [322]. The shape of graphene flakes can also be influenced by the gas conditions. Initially, square-shaped graphene domain can be controlled by growth conditions, e.g., methane partial pressure [323], regardless of the Cu lattice orientation. Generally, a high hydrogen flow ratio (in comparison to methane pressure) facilitates hexagonal graphene [206, 316], while low hydrogen partial pressure facilitates square graphene domains. Moreover, annealing with high-partial pressure H_2 single gas can etch the square-shaped graphene flakes into hexagons [206].

Reaction mechanism over Ni

Ni as a substrate for graphene growth exhibits carbon segregation and precipitation [216, 218, 324]. Initially, in a CVD reaction, carbon atoms dissolve [325] into the Ni bulk forming a carbide [326]. Carbon segregation and precipitation from meso-stable Ni_2C [327] occur upon cooling. However, graphene grown on pure Ni foil is

inhomogeneous in layer numbers, ranging randomly from 1 to 10 layers.

Therefore, one needs to engineer the substrate to achieve homogeneous graphene layer formation. One example is to employ Ni thin films to decrease the quantity of carbon that can diffuse into the Ni [216, 328]. Furthermore, mild oxidants (CO_2 and H_2O) can be mixed with methane to grow thin few-layer graphene with diminishing carbon diffusion [324] because Ni sub-oxide not only increases catalytic activity but also leads to the suppression of carbon diffusion. Graphene growth over NiOx with CO_2 enhancement is shown in Fig. 2.

Alternatively, when using a binary alloy (Ni/Mo) [188, 190], one can produce strictly monolayer graphene. Figure 3 shows a monolayer graphene growth on an Ni–Mo alloy. Similarly to Ni/Mo alloy, one can control the graphene layers from monolayer full film to a bilayer full membrane by tuning the component ratio of Cu/Ni alloy [189].

Reaction mechanism over non-metals

Graphene growth can also be achieved over non-metal substrates, for example Al_2O_3 [223], MgO [225], and SiO_2 [210, 222]). In comparison to Cu CVD, the growth over oxides generally requires higher temperatures >1100 °C, [210, 222]. In addition, surface oxygen [210], metal vapor [209, 329], and plasma [229] are necessary to promote graphene growth.

Graphene growth over sapphire (Al_2O_3) involves epitaxial growth by van de Waals interactions [223]. The unit cell of the grown graphene has a 30° rotation compared with that of sapphire substrate. High-resolution TEM (see Fig. 4) proves the parallel stacking of graphene over MgO crystals [225], which also confirms epitaxial growth. In addition, graphene was successfully grown over non-metal crystalline substrates such as graphite [330, 331], SiC [187], BN [226, 228], and graphene on a Cu support [13].

The growth mechanisms over non-metals are not yet clear. The graphene growth is argued to involve a surface deposition mechanism with a very slow deposition rate [210]. A vapor–solid–solid mechanism is also argued [210, 222]. SiO_2 nanoparticles were suggested to nucleate graphene growth [210] probably through an intermediate of SiC formation [281]. Without any treatment of oxide substrates, the grain size of graphene is small, around 300 nm [210]. However, with a pretreatment of air

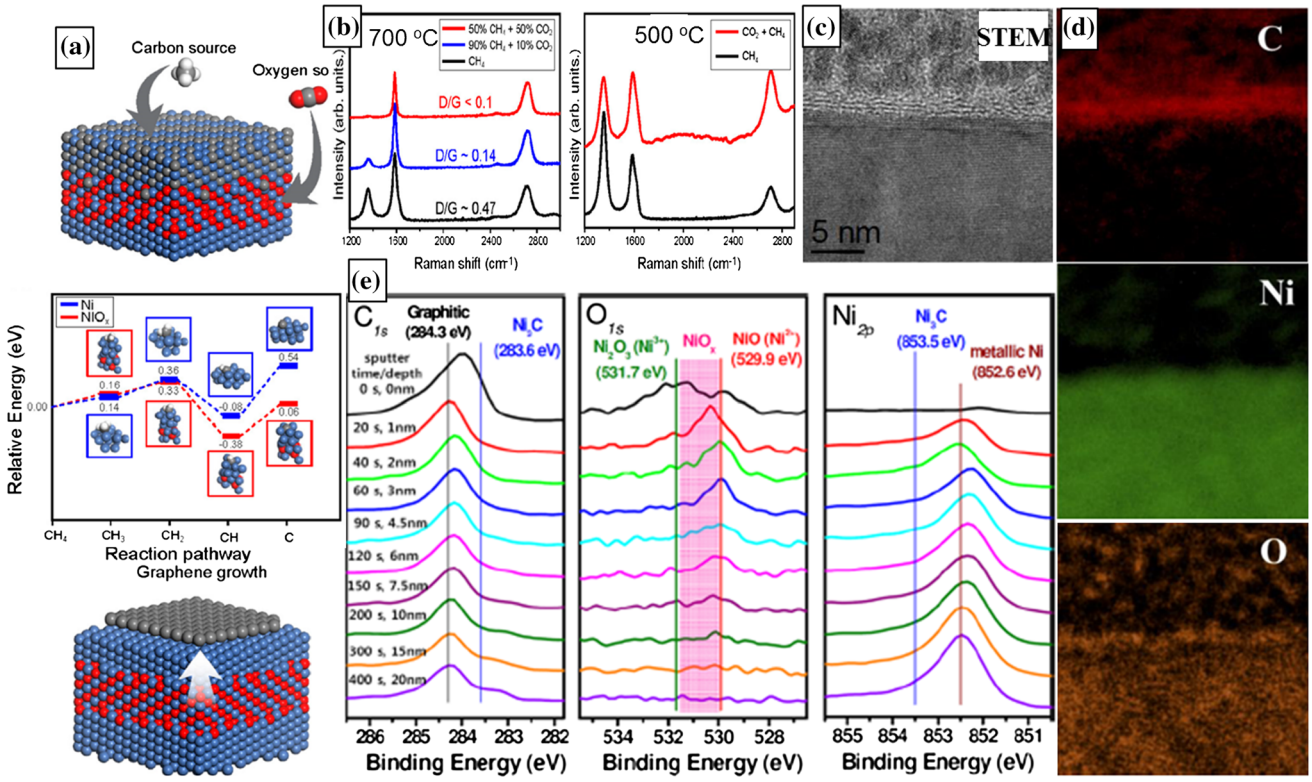

Fig. 2 Graphene growth on NiO_x substrate with CO_2 enhancement. **a** Schematic of CVD growth of graphene over NiOx surface. Middle is the energy state versus the reaction pathway of methane dissociation. **b** Raman spectra of graphene grown at 700 and 500 °C with/without CO_2 incorporation. With CO_2, the D mode decreases. **c**,**d** STEM image and EDX mapping of C, Ni, and O in a cross section of graphene/NiOx interface. **e** XPS of the surface of graphene over NiOx. There is direct observation of oxygen at top surface of the Ni substrates. Reprinted (adapted) with permission from Ref [324]. Copyright (2014) American Chemical Society

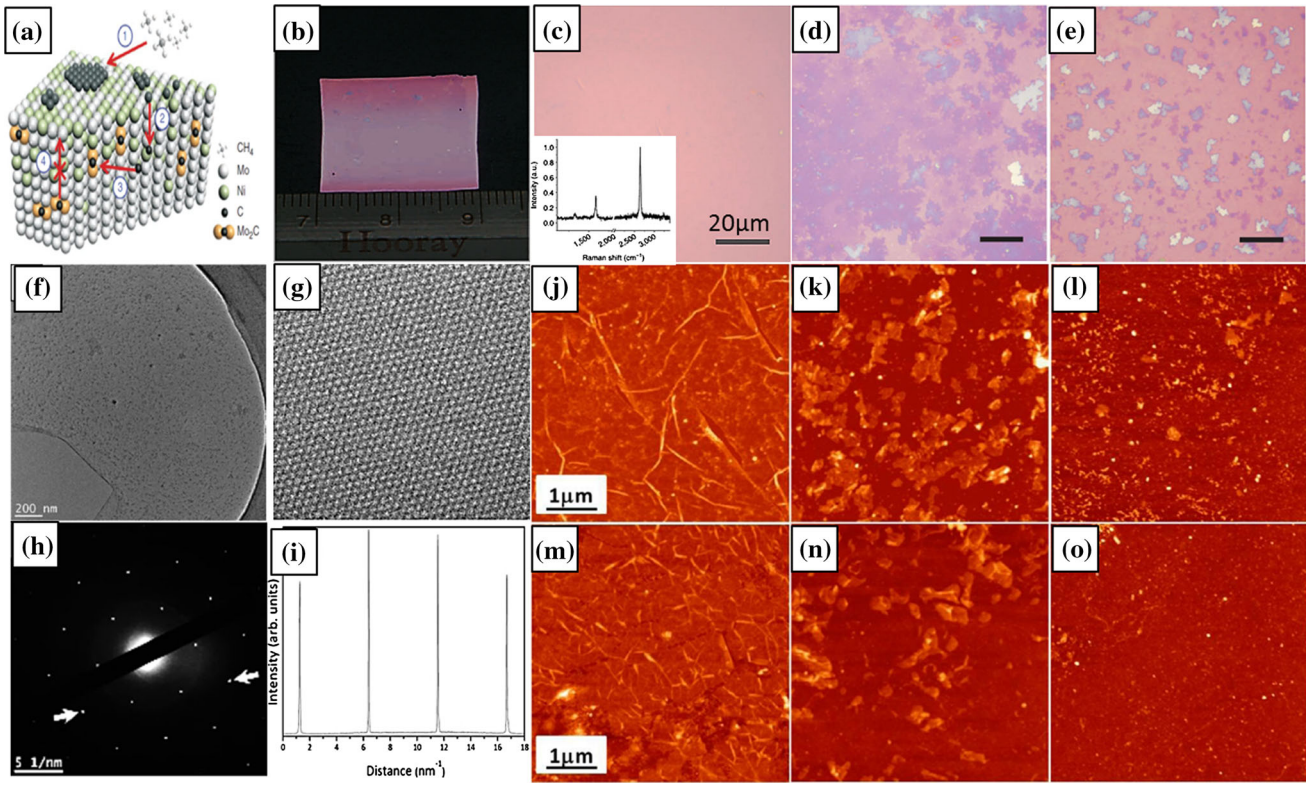

Fig. 3 Monolayer graphene growth from Ni–Mo binary alloy. **a** Schematic of growth mechanism: surface decomposition of carbon feedstock, carbon atoms' dissolution into the bulk, Mo_2C formation, and controlled carbon precipitation into graphene. **b** Photograph of full coverage graphene film transferred onto Si/SiOx substrates. **c** Optical micrograph of the transferred full coverage graphene, *inset* is typical Raman spectrum that confirms the monolayer graphene feature. **d**,**e** Discontinuous graphene film and graphene flakes with slow cooling rate after CVD. Adapted by permission from Macmillan Publishers Ltd: [Nature Communications] [188] copyright (2011). **f**–**i** TEM characterization of the graphene monolayer membrane. **j**–**o** AFM height images of the transferred graphene on Si/SiOx. From left to right are the evolution of monolayer full film, discontinuous film, and isolated flakes, according to various cooling temperature windows. Reprinted (adapted) with permission from Ref [190]. Copyright (2013) American Chemical Society

annealing, the graphene size exceeds 10 microns [222]. The growth kinetics is probably limited with slow carbon attachment at graphene edges [222]. Si_3N_4 is also a candidate substrate for graphene growth [224].

The growth mechanism of vertical graphene is shown in Fig 5. The defects of initial graphene sheets supply the nucleation sites. Then, the graphene continues to grow with surface diffusion of active carbon species.

Transfer protocol

Graphene grown on metals requires a transfer step for further characterization or device fabrication. Firstly, the graphene side is (spin-) coated with a supporting film, usually a polymer such as PMMA [216, 332, 333]. Secondly, the polymer/graphene/Cu stack is put afloat on an etching agent, such as $FeCl_3$ [333] and ammonium persulfate (APS) [334, 335]. Thirdly, the polymer/graphene is cleaned in distilled water after thorough etching of the metal. Then, the polymer/graphene is fished onto a target substrate. Next, acetone is used to dissolve the polymer (e.g., PMMA) away. Finally, the transfer process is completed with high-vacuum annealing to minimize surface contamination. When the annealing temperature exceeds 300 °C, the electric property improves with negligible polymer residues [335]. In addition, the graphene on the undesired side of a substrate or foil can be pre-etched away with nitric acid [335] or APS [334] since graphene can grow on both sides of a foil/substrate. We list the transfer protocol and the chemicals for each step in Table 3.

Alternative approaches for graphene transfer also exist. Bubbles can be used to intercalate into the interface between the graphene and the substrate and thus separate them. The bubbles are usually generated in an electrochemical reaction [338]. To recycle Cu foil, an electrochemical cell is used in a controlled fashion to dissolve a very thin layer of Cu (cathode) underneath the graphene [338, 339]. In this mild etching, hydrogen bubbles from the electrolysis of water can assist in peeling off the PMMA/graphene from Cu.

A bubble method was successfully developed that does not require an electrochemical cell and so can be applied to

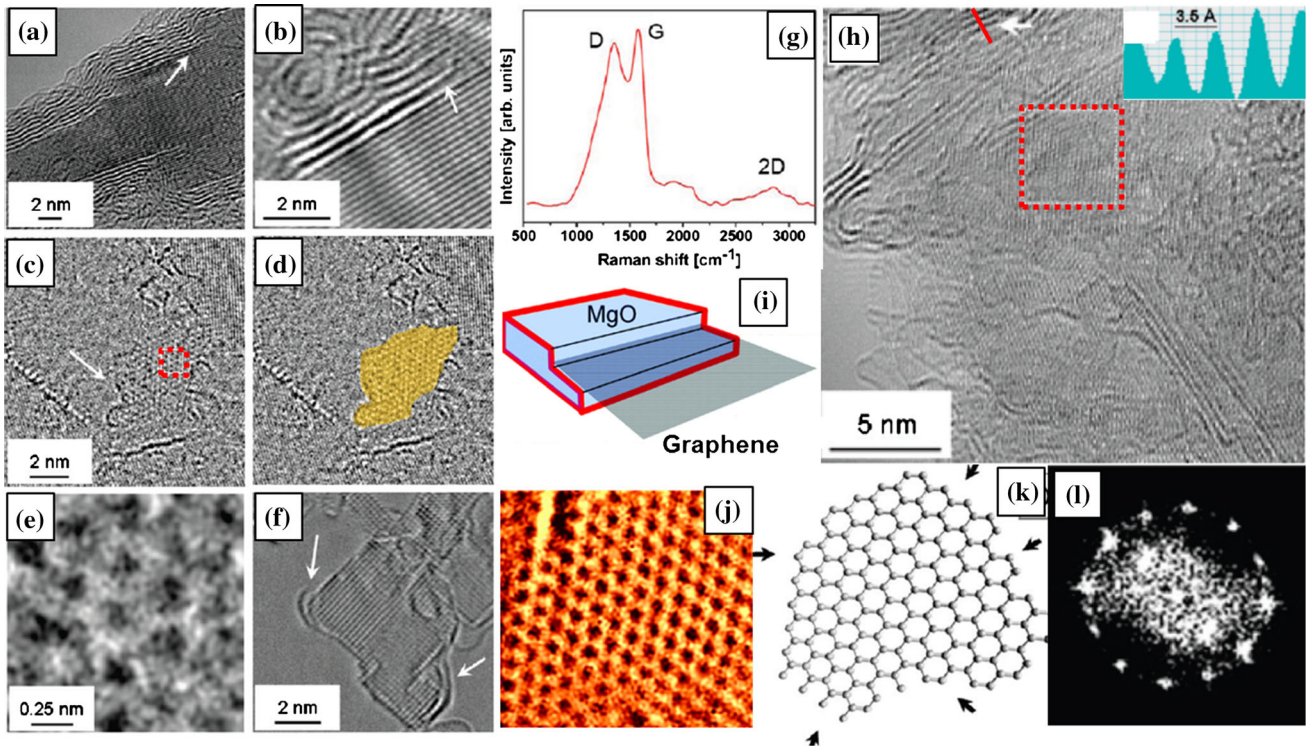

Fig. 4 Graphene grown on MgO substrate. **a**,**b** TEM images of few-layer graphene on MgO lattice. **c**,**d** Graphene nano-flake on MgO surface with short exposure of carbon feedstock. **e** Magnified region from *panel c* highlights the graphene structure. **f** Cross-sectional view of graphene on MgO surface. **g** Raman spectrum of few-layer graphene after purification. **h** TEM of the purified graphene. *Inset* is the contrast profile of graphene interlayers. **i** Scheme of graphene growth on MgO: nucleation at the step edge. **j** HRTEM of magnified region of *panel c*. **k** Schematic of a nanographene flake illustrating the large number of edge defects. **l** Fast Fourier transform images from magnified region in *panel h*. Reprinted (adapted) with permission from Ref [225]. Copyright (2010) American Chemical Society

non-conductive substrates [337]. The process relies on the copious production of gaseous O_2 which intercalates in between the substrate–graphene interface and can thus serve as a peeling agent. The schematic is shown in Fig. 6.

Mechanical transfer can be achieved by peeling off sticky epoxy/graphene from a substrate [341]. In a similar manner, thermal release tapes in a roll-to-roll dry transfer route can separate graphene from a support [219].

Alternative polymers such as polycarbonate (PC) [336] can be used to diminish polymer residue. PC polymer dissolves more effectively in chloroform than the PMMA/acetone combination. This can avoid the need for high-vacuum annealing. The use of fluoropolymers (CYTOP model) instead of PMMA can achieve fluorine doping in graphene [342]. This single step largely increases the electrical conductivity (with higher carrier density) but preserves the high transparency of the graphene. When fishing a polymer/graphene stack out of water onto a substrate, isopropanol is a better medium than water to guarantee better adhesion over the Si/SiO_2 substrate [343]. However, without a polymer support, graphene can be directly fished onto a net upon Cu removal [340].

In terms of graphene over In or Ga, HCl solution can be used as an etching agent [204, 318]. For graphene on Ni, the etching agent can vary from mild hydrochloric acid [216], acetic acid [18, 19], O_2 bubbles [337], and nitric acid [18]. In the case of oxide-based supports, HCl was employed to remove MgO nanocrystals [16]. KOH can etch SiO_2 substrates (such as quartz or amorphous SiO_2 film) [344, 345].

CVD growth of carbon nanotubes

The primary approaches to synthesize CNTs are arc-discharge evaporation of graphite, laser ablation, and CVD. In particular, CVD is well developed in industry and easier to scale up than arc-discharge and laser evaporation methods. Hence this section is focused on CVD growth of CNTs. The CVD approaches discussed here are divided into two sections, catalyst CVD and catalyst-free CVD [2, 346].

Substrate pretreatment

Prior to the CVD growth of CNT, the substrates often requires pretreatment. Air annealing at 400–750 °C is

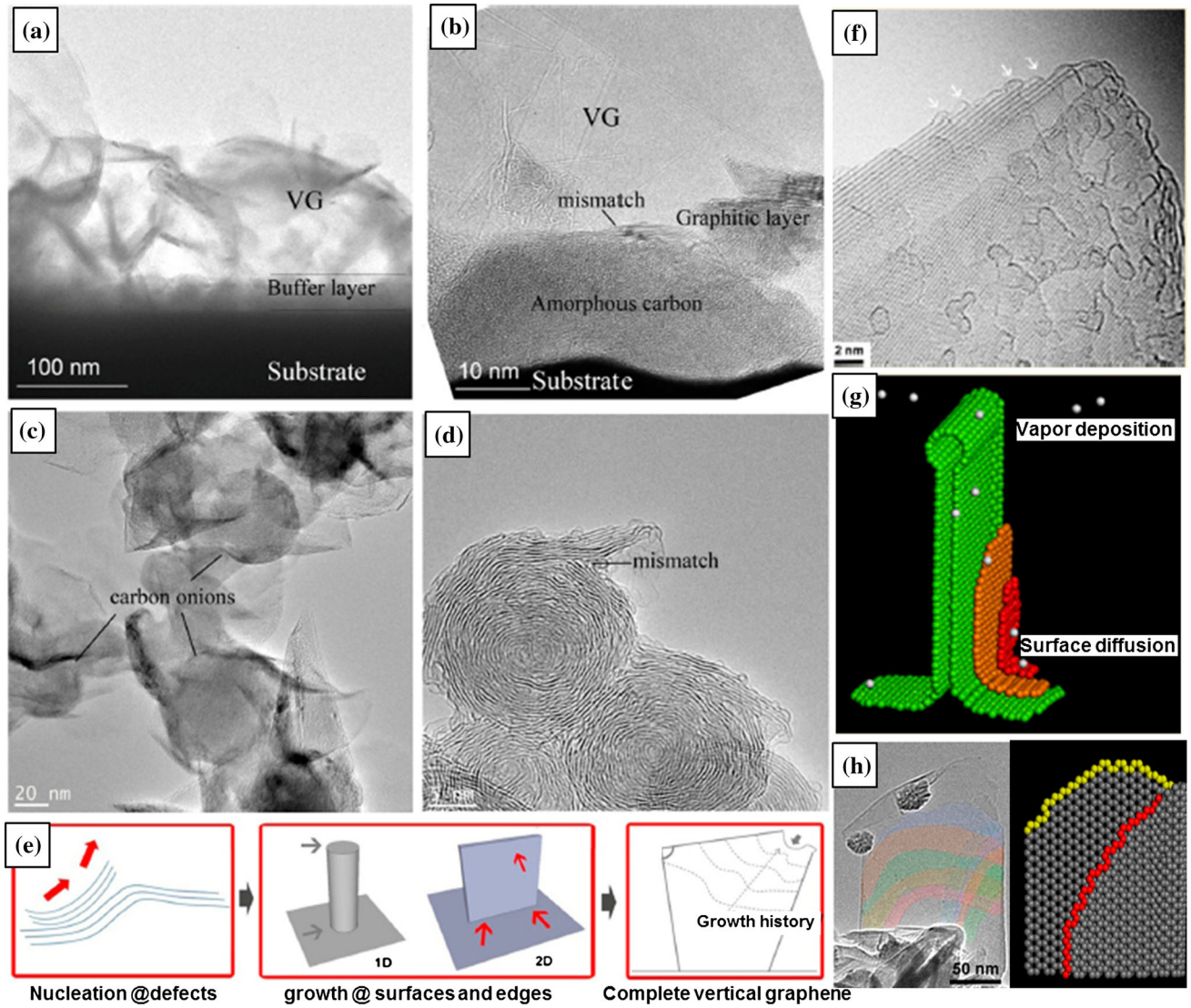

Fig. 5 Vertical graphene (VG) grown from PECVD. **a** Low-resolution TEM images of VG including graphene top, bottom, and substrates, **b** high-resolution TEM image of VG bottom. The mismatches are probably nucleation sites. **c** HRTEM of VG stems on carbon onions. **d** HRTEM of the carbon onion. **e** Scheme of a proposed mechanism: nucleation at defects, growth at surface and edges. **f** HRTEM of a seamless edge of a graphene closure. **g** Schematic of the vertical graphene growth at its closure. **h** TEM and atomic model of a growing VG sheet with many curved steps and terraces. Reprinted (adapted) with permission from Ref [23]. Copyright (2014) American Chemical Society

Table 3 Transfer protocol for graphene over Cu

Etching of bottom graphene	Coating polymer support	Etching Cu	Fishing graphene onto substrate	Removal of polymer	Ref.
APS	PMMA	$FeCl_3$/HCl	Water	Acetone	[216, 332–334]
HNO_3	PMMA	APS	Isopropanol	Acetone	[335]
No	PC	$FeCl_3$	Water	Chloroform	[336]
No	PMMA	$H_2O_2 + NH_3{\cdot}H_2O + H_2O$	Water	Acetone	[337]
No	PMMA	Electrochemistry	Water	Acetone	[338, 339]
No	No	APS	No	No	[340]

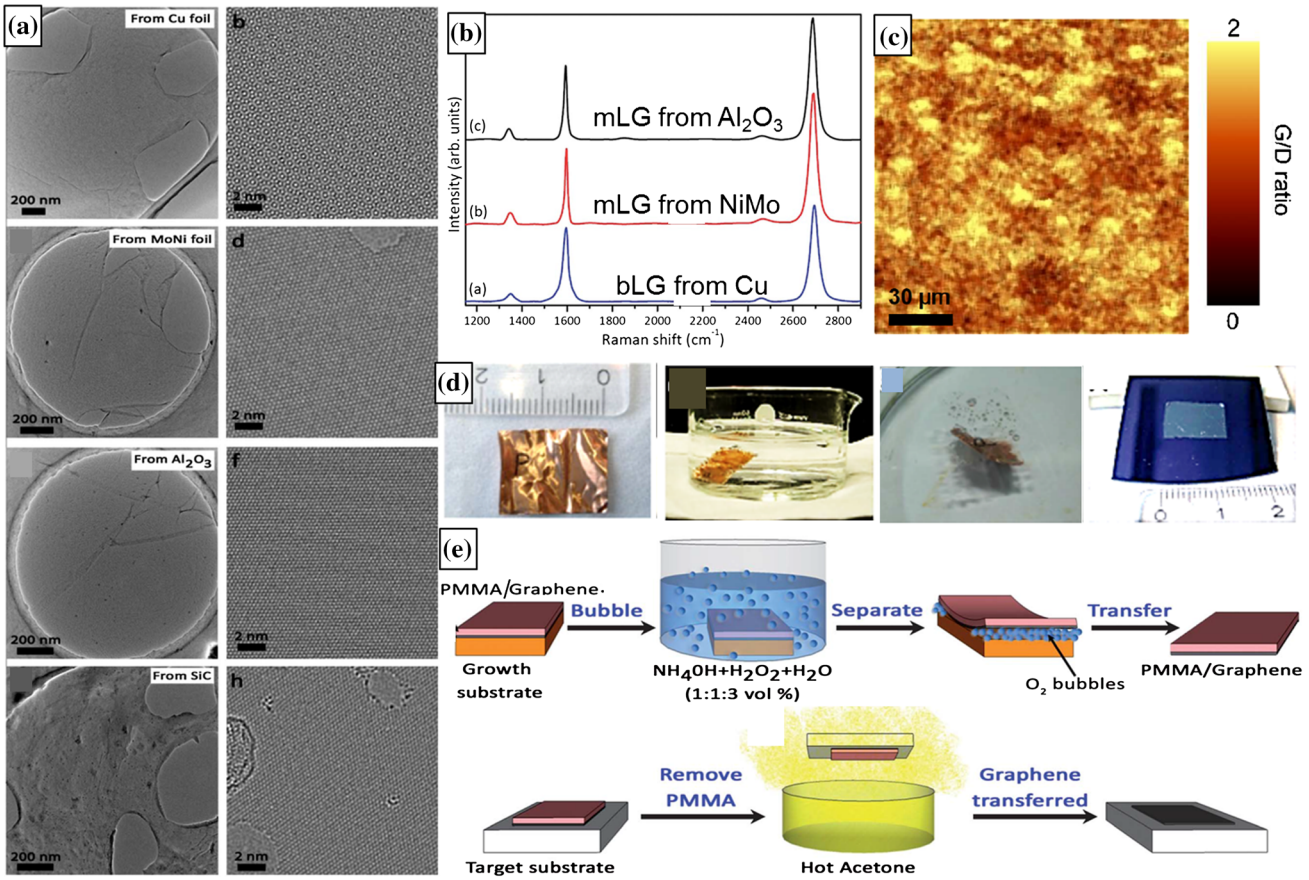

Fig. 6 A bubble approach to transfer graphene from arbitrary substrates. **a** TEM micrographs of graphene transferred to a grid from Cu, Ni–Mo, Al_2O_3, and SiC substrates. **b** Raman spectra of transferred graphene. **c** Raman mapping of G/D mode of graphene transferred from Cu foil. **d** Photographs of key steps of the transfer: coating PMMA, immersion into bubble agents, and delaminating PMMA/graphene with Cu foil. **e** Schematic of the complete transfer route. Reprinted (adapted) with permission from Ref [337]. Copyright (2014) Royal Society of Chemistry

widely used. This process can oxidize the metal particles (catalyst particles) which minimizes Oswald ripening at the elevated temperatures used in the reaction. In addition, organic contaminants can be removed [347]. Moreover, long air annealing times can reduce substrate roughness [348]. Indeed, substrates with a rough surface can halt CNT growth or lead to twists the growth direction and is sometimes implemented for horizontally aligned CNT growth.

Catalyst chemical vapor deposition

The more common catalysts used in the CVD growth of CNT are Fe, Co, and Ni or related alloys [2, 346]. There are two types in catalyst systems in CNT production by CVD. They are the floating catalyst CVD and supported CVD. In the floating catalyst system, the catalysts are not supported and reside in the gas flow [349, 350]. In supported catalysis, nanoparticles are pre-deposited on supporting substrates and serve as the catalyst particle. According to the CVD conditions implemented, one can obtain three types of CNT orientations. They are vertically aligned CNT [351, 352], horizontally aligned CNT [353–357], and randomly aligned CNT [358].

Catalyst-free chemical vapor deposition

Non-catalysts such as ceramic oxides have been shown to grow CNT [346]. In addition, carbon allotropes, such as fullerenes [271, 354], diamond surfaces [359], graphite [271], and CNT [360, 361] are successful systems to synthesize CNTs.

Growth mechanisms

Thermodynamics and activation energy

The thermodynamics (e.g., activation energy) to grow CNTs has been carefully studied over various conditions

[362–366]. Table 4 provides a comparative overview of the parameters that affect activation energy. In this review, thermal CVD and PECVD are compared. For thermal CVD, the Ea of CNT growth can be as high as 1.21 eV (Ni–C_2H_2) [364]. In contrast, PECVD significantly reduces the Ea, e.g., 0.56 eV [363] and 0.76 eV (Ni–C_2H_2) [364]. These values are obtained in the temperature range (520–700 °C). Plasma CVD has benefits at low temperatures. For example, one could grow device-quality CNTs at 200 °C [367] with the plasma-assisted CVD. This allows CNT vertical arrays to be directly grown on a plastic polyimide substrate.

Many factors account for the lower Ea in PECVD than a thermal CVD [364]. Firstly, the catalytic particles could be heated by ion bombardment and increase the carbon diffusivity and solubility within them. Secondly, the activated etching gases could more effectively remove excess carbon species from the front nickel surface, and thus an enhanced uptake of carbon occurs at the larger fresh area of the metallic catalyst particle. Both factors could provide a driving force to allow carbon diffusion through the catalyst particles.

In terms of the role of the catalyst metal choice, the highest Ea is 3.5 eV for Co–C_2H_2 couple [366]. With Ni and Fe employed, the Ea drops significantly to 2.3 eV [366] and 1.3 eV [365], respectively. Indeed, the same trend occurs when using C_2H_4 as the feedstock gas. They are Co (1.69 eV) [362] and Ni (1.4 eV) [366]. However, a complex alloy of Co/Cr/Al [362] significantly suppresses the Ea barrier to 0.84 eV.

We now turn to the influence of carbon feedstock. When mixing a promoting gas such as NH_3, the Ea (1.21 eV) [364] for Ni–C_2H_2 (NH_3) decreases to half of that found with Ni–C_2H_2 (2.3 eV) [366] at ambient pressure. Different feedstocks with Ni catalyst, such as CH_4 (1.5 eV), C_2H_4 (1.4 eV), and C_2H_5OH (1.3 eV), lead to varying activation energies. Co catalyst particles show a similar trend when switching from C_2H_2 (3.5 eV) [366] to C_2H_4 (1.69 eV) [362] and C_2H_5OH (1.1 eV) [366].

In thermal CVD growth, Ea tends to be larger (1.1–3.5 eV) in low-temperature zones (<600–700 °C) and much smaller (0.1–0.7 eV) in high-temperature zones(>600–700 °C) [366]. The decrease of Ea probably depends on the liquefaction of the metal catalyst particles. At elevated temperatures, the nano-sized metal catalysts liquefy at lower temperatures than their bulk counterparts [270, 368–371]. The activity of catalyst particles can be enhanced upon increasing the temperature. Indeed, molten

Table 4 Activation energy of carbon nanotube growth over various substrates

(Catalyst) particle type	Ea (eV)	Carbon feedstock	CVD type	Temperature (°C)	CNT type	Ref.
Co	3.5	C_2H_2	Thermal CVD	450–700	SWNT	[366]
Ni	2.3	C_2H_2	Thermal CVD	450–600	SWNT	[366]
Co	1.69	C_2H_4	Thermal CVD	500–700	MWNT	[362]
Ni	1.5	CH_4	Thermal CVD	450–625	SWNT	[366]
Ni	1.4	C_2H_4	Thermal CVD	450–625	SWNT	[366]
Ni	1.3	C_2H_5OH	Thermal CVD	450–680	SWNT	[366]
Fe	1.3	C_2H_2	Thermal CVD	600–800	MWNT	[365]
Ni	1.21	C_2H_2/NH_3	Thermal CVD	550–850	MWNT	[364]
Co	1.1	C_2H_5OH	Thermal CVD	450–700	SWNT	[366]
Co/Cr/Al	0.84	C_2H_4	Thermal CVD	500–650	MWNT	[362]
Ni	0.76	C_2H_2/NH_3	PECVD	550–850	MWNT	[364]
Ni	0.7	CH_4	Thermal CVD	625–900	SWNT	[366]
Ni	0.56	C_2H_2/NH_3	PECVD	520–700	MWNT	[363]
Ni	0.4	C_2H_2	Thermal CVD	600–900	SWNT	[366]
Co	0.4	C_2H_5OH	Thermal CVD	700–900	SWNT	[366]
Fe	0.35	C_2H_2/NH_3	PECVD	260–520	MWNT	[373]
Ni	0.32	C_2H_5OH	Thermal CVD	680–900	SWNT	[366]
Ni	0.3	C_2H_4	Thermal CVD	625–900	SWNT	[366]
Co	0.3	C_2H_2/NH_3	PECVD	200–520	MWNT	[373]
Ni	0.23	C_2H_2/NH_3	PECVD	120–520	MWNT	[373]
Co	0.1	C_2H_2	Thermal CVD	700–900	SWNT	[366]

particles continue adsorbing carbon atoms and elongating (growing) nanotubes after nucleation. However, as the liquefaction temperature increases beyond the synthesis temperature, the carbon concentration increases in the metal particles [372]. Solidification decreases the carbon diffusion kinetics and finally ceases CNT growth altogether.

Similarly, in PECVD the Ea varies between two temperature regimes. The Ea is larger (0.76 eV) [364] at high temperatures (520–700 °C) but smaller (0.23 eV) [373] at low temperatures (120–520 °C). Indeed, the Arrhenius plot has a strict linear fitting at the low temperature range [373]. A linear fit occurs only in the low portion in the high-temperature zone [364].

One can engineer the kinetics of CVD with predictions (rather than trial-and-error mode) [374]. For example, the CNT synthesis can be conducted with a controlled diameter [375–378] or even reasonably defined chirality [379–381]. Moreover, the kinetic process of CNT formation can be monitored with enriched in situ characterization techniques, such as digital camera [382], reflection optical spectroscopy ([383, 384]), adsorption optical spectroscopy [385], Raman spectroscopy [386–389], thermogravimetric analysis [288], XRD [390], XPS [391], and environmental TEM [82, 392–394].

The termination of CNT growth is controversial. Early work deduced that the growth ceases upon the deactivation of the catalyst particles. The deactivation includes the poisoning of catalysts by amorphous carbon encapsulation [395–397], or by Oswald ripening/sub-diffusion [398]. This theory is elegantly supported by the water-assisted super growth of vertical CNT arrays [351, 399, 400]. Indeed, water incorporation at elevated temperature removes the amorphous carbon layer and exposes the fresh catalyst surface [398]. Thereafter, the catalysts re-activate for the CNT growth. Similarly, oxidants such as O_2 and CO_2 show an enhancement in SWNT growth [400]. Moreover, oxidized substrates may drive CNT growth by preventing amorphous carbon condensation [80]. But, one convincing argument rises up for the non-poisoning nature of amorphous carbon layer [401]. Here, amorphous free radical condensates over catalyst are proposed to serve as a carbon source rather than a deactivation system. Indeed, high-resolution TEM shows that the amorphous carbon covering catalyst can continue CNT growth [402]. Beyond these two arguments, vertical CNT arrays show a genuine saturated growth behavior [403, 404].

Reaction mechanism over catalysts

The reaction mechanism over catalysts include carbon dissolution and nanotube precipitation [2, 346]. Depending on the catalyst particle location, the growth mechanisms are divided into tip growth mode (where particle rises to the top) and base growth mode (where catalytic particles anchor to the supporting substrate). Ni over SiO_2 often follows tip growth because of a weak particle–substrate interaction [80, 363]. However, Co and Fe over SiO_2 substrates [405, 406] and over Al_2O_3 [78] favor base growth where a strong interaction limits the motion of the catalyst particles. Indeed, over Al_2O_3 support, the catalyst particles were found either embedded inside the supporting film or anchored on its surface (see Fig. 7).

The reaction to form MWNTs over Ni includes (1) decomposition of carbon feedstock on the front face of a catalyst particle; (2) carbon dissolution and supersaturation in the bulk metal particle; (3) carbon precipitation to the back face; and (4) carbon incorporation at the root of a growing CNT. During the CNT growth, the Ni particle is raised upward spontaneously. The driving force to continue growth dynamics originates from the gradient in chemical potentials [407–409], particle temperature gradients (front face > back face), and carbon concentration gradients (front face > back face). Namely, carbon (monomers or dimers) diffuses from high to low temperature and from high to low concentration in Ni particles. In terms of SWNTs, a carbon dissolution and nanotube precipitation mechanism applies. But, the driving force relies solely on the gradient in carbon concentration since the temperature difference is negligible in a sub-10 nm particle [410, 411]. To obtain SWNTs, one needs to optimize a number of parameters [2, 289, 412, 413], such as catalyst choice, temperature, and feedstock.

Diameter control of SWNTs can be achieved by various strategies, for example, using sulfur-promoted aerosol-assisted CVD [375], or to confine the catalyst particle size with secondary non-catalytic metals (such as Mo, Pt, Ru, Rh, and W). Thus, binary alloys such as Co/Mo [412, 414],Fe/Mo [413, 415, 416], and Co/Pt [417] are often used confine SWNT growth to the base growth mode. Furthermore, water incorporation (or other mild oxidants) help prevent Oswald ripening of Co over Mo, therefore narrowing down the diameters of the resultant SWNT [414]. Surprisingly, some degree of chiral control of SWNTs via CVD is emerging such as (12,6) tubes from Co/W clusters [418], (9.8) tube from $CoSO_4/SiO_2$ [419] and from Co/TUD-1 [420], cloning of (7,6) and (7,5) tubes [360], and (6,5) tube over Co_xMgO substrates [421] and from Co/Pt catalysts [417].

In an atomic view, a theory of screw dislocation has been postulated for chiral SWNT growth [422]. In this work, the SWNT grows with C monomer attachment along the exposed tube edge in a screw-like fashion. Surprisingly,

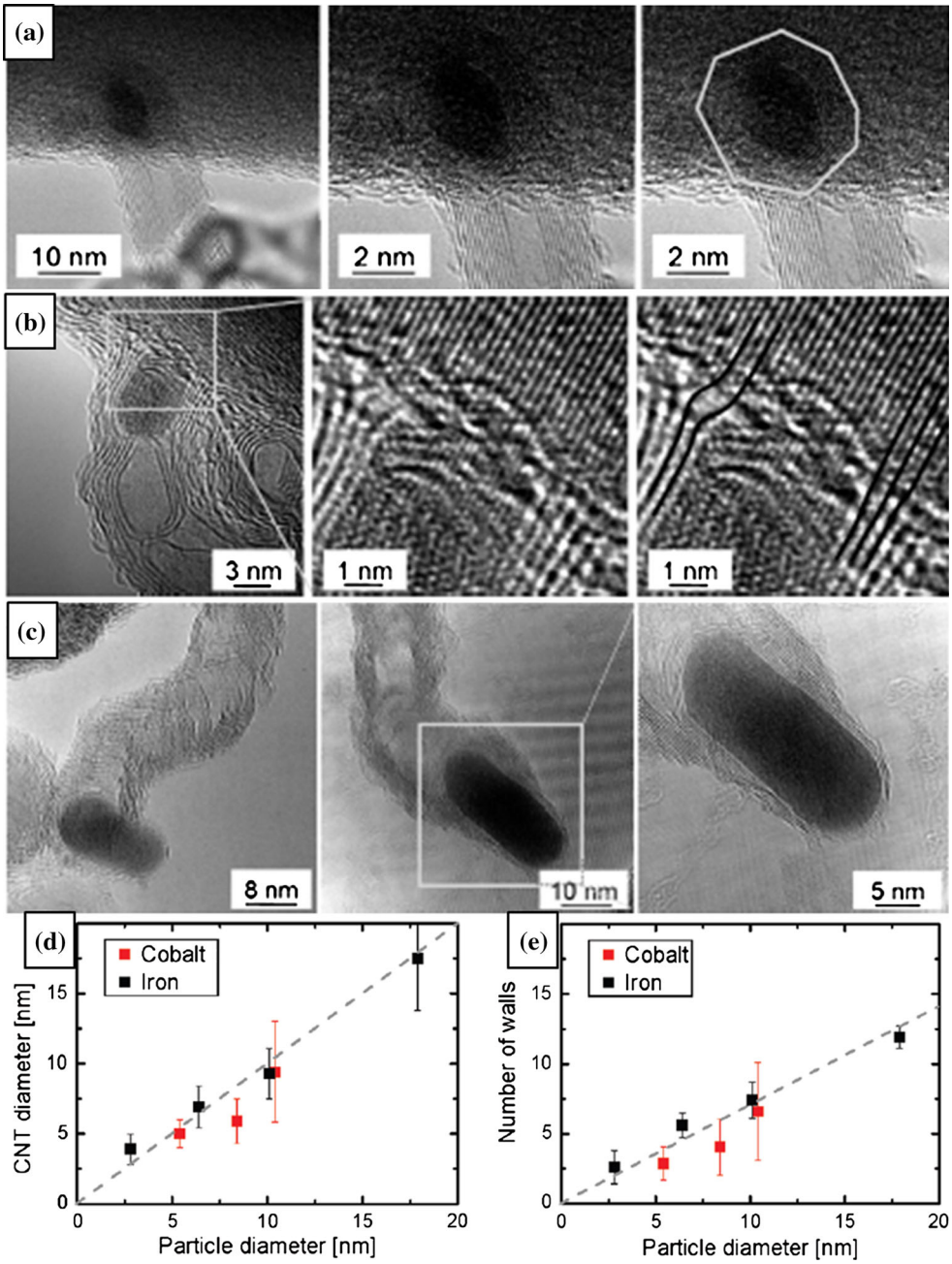

Fig. 7 Carbon nanotube (CNT) growth on various supports. **a** TEM images of CNT with root on the surface of Al_2O_3 thin film while catalyst buried inside the Al_2O_3 film. **b** TEM images of CNT with root on α-alumina nano-platelet. A Co particle elongates inside the CNT. The outer walls of CNTs align themselves with the (110) lattice fringes of the corundum support. **c** TEM micrographs of bamboo-like CNT grown on a graphite support. The right *panel* highlights the graphitic cap terminating the outside of catalyst particle. Correlation of CVD grown CNT diameter with catalyst particle size (**d**) and number of CNT walls with respect to catalyst particle size (**e**). Reprinted (adapted) with permission from Ref [78]. Copyright (2010) American Chemical Society

the screw theory has been confirmed with experimental observations under a field emission microscopy [379].

Reaction mechanism over non-metals

Table 5 summarizes different aspects of CNT growth from non-catalyst, mainly non-metals. CNT growth from carbon allotropes usually arises from defects such as nano-pores, open edges, and defects. Indeed, the exposed open edges of CNT walls (such as bulky onions and stack mismatches [23], Fig. 5) between graphitic sheets can facilitate the attachment of carbon adatoms [379]. On the one hand, the open-end tube structure has a high-energy state, which can crack carbon, the feedstock. These carbon atoms could initialize the formation of MWNTs or SWNTs depending on the size of the nuclei site. On the other hand, the defect sites or particle encapsulates (similar to Ni particle at tip) [396] may continue supplying sites to template the elon-

Table 5 Growth conditions and results of CVD-grown CNTs, support type, curvature radius, and diameter of CNTs, nucleation site, CNT type, and particle location

Support type	Particle radius (nm)	CNT diameter (nm)	Nucleation sites	CNT type	Particle location	Ref.
Fullerene clusters	1–4.5	0.7–1.4	Open cap	SWNT, DWNT	Base	[354, 423, 424]
SWCNT	1	2	Open end	SWNT	None	[361]
MWCNT	12	25	Pore site	MWNT	None	[272]
Graphene quantum dots	20	20	Mismatch between graphene sheets	MWNT	None	[425]
Graphite	20–40	20–90	Nanobump	MWNT	None	[271]
Diamond nanoparticle	2–2.5	1–2	Graphitic cap	SWNT	Base	[359]
Porous carbon black	10–40	20–80	Fullerene-like cap	MWNT	Base	[272]
Si, Ge nanoparticle	0.7–0.9	3–4	Nanoparticle	SWNT, DWNT	Base	[426]
SiC nanoparticle	0.6	3–4	Nanoparticle	SWNT, DWNT	Base	[426]
Nanoparticles SiO_2, Al_2O_3, TiO_2, ZrO_2	<1	0.8–1.4	Nanoparticle	SWNT	Base	[357, 427–432]
SiO_2 powder	4-10	15–18	SiC nanoparticle	MWNT	Both	[281]
MgO powder	25	50–300	Defected Graphene shell	MWNT	Tip	[433]
ZnO nanoparticles	0.8	0.6–1.8	Nano particle	SWNT	Tip	[434]
Au (bulk)	5-50	25–60	Hemi-spherical nanobug	MWNT	Base	[435]
Ag, Pt, Pd, Mn, Mo, Cr, Sn, Mg, Al, Cu, Au,	n.a.	0.6–2.0	Nanoparticle	SWNT	n.a.	[344, 436–439]
Pt	0.5-1.5	0.8–1.2	Sub-surface	SWNT	n.a.	[440]
Re	2-4	5–8	Nanoparticle	MWNT	Tip	[441]
NaCl, Na_2CO_3, Na_2SO_4	10	8–23	Encapsulated particle	MWNT	Tip	[442]

gation. When expanding to other non-carbon particles, the initial nucleation occurs by forming carbon nano-caps.

Other elements such as Si, Ge, and SiC can also serve as catalyst particles for the growth of CNT. The Ge particle is proposed to be a liquid during growth. In contrast, Si and SiC are argued to be solid during growth.

SiO_2 nanoparticles have also been used to grow CNTs (Fig. 8). When SWNT grows out from nano-SiO_2 particles, SiO_2 is assumed to be either a liquid [428] or an amorphous solid [357, 429] during the reaction. However, these hypotheses were deduced with micro-meter-scale resolution methods, like XPS.

Many metal oxides [357, 427–433] such as Al_2O_3, TiO_2, ZrO_2, ZnO, and MgO have also been used for CNT growth.

Low catalytically active metals such as Au, Cu, Pt, Ag, Pd, Mn, Mo, Cr, Sn, Re, Mg, and Al [344, 436–439] have also been used for CNT fabrication. Last but not least, alkali salts [442] such as NaCl and Na_2CO_3 have also been demonstrated for the growth of CNT.

Conclusions

In this work, an overview of the CVD aspects involved in the synthesis of graphene and CNTs have been presented for both thermal and plasma-enhanced CVD. The shear breadth of possibilities is highlighted by the number of variations available in terms of the presence of catalyst, synthesis parameters, feedstock options, etc., all of which affect the thermodynamics and kinetics of the reaction and hence the final outcome of the as-produced material. The review highlights the enormous power of CVD as a synthesis route for graphene and CNTs as well as its versatility. Despite some remaining technical issues such as grain boundary control in large-area graphene or total chiral control of carbon nanotubes, the sheer volume of knowledge now available and recent advances suggest the use of CVD as a means to fabricate graphene and CNTs are not only set to stay, but will likely soon overcome many of the remaining technical challenges and thus allow graphene and CNTs to truly deliver their full promise.

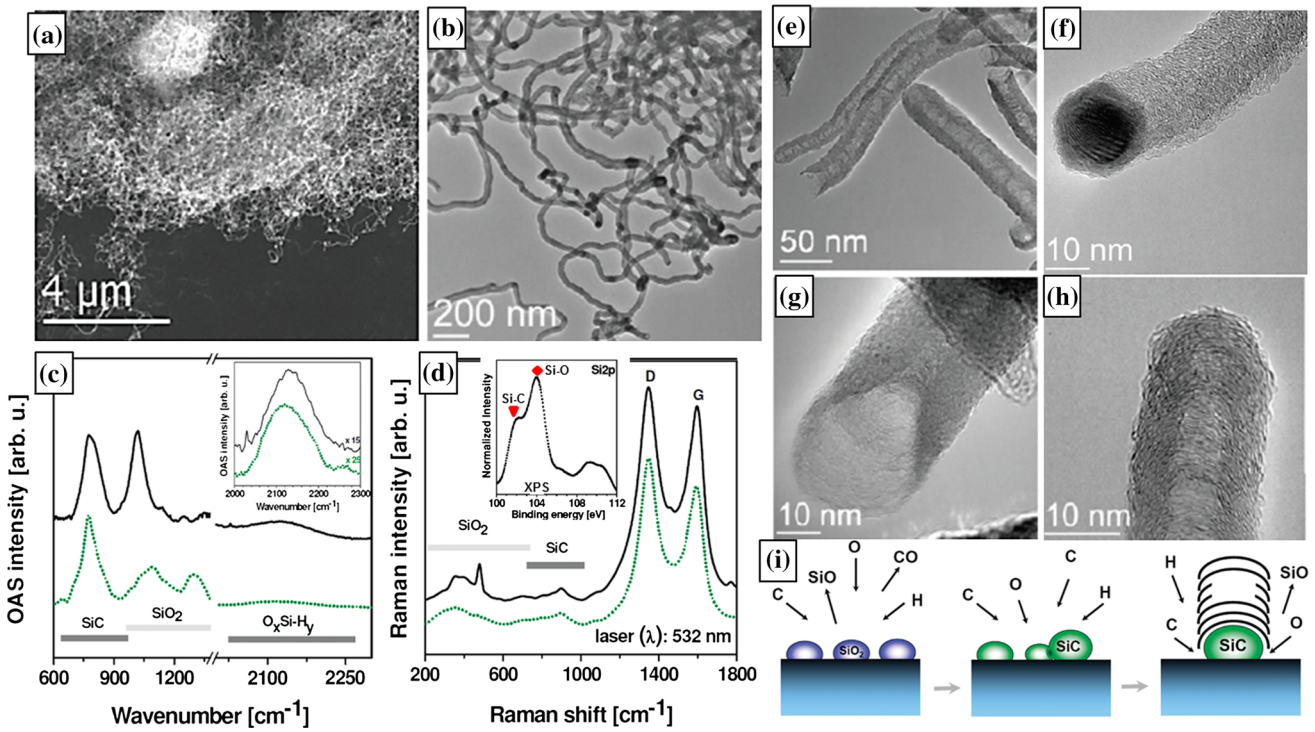

Fig. 8 Carbon nanotube growth over SiO_2 support without a catalyst. **a** An overview with SEM graph of dense CNT networks. **b** Low-resolution TEM images of the CNTs. **c** Optical absorption spectra of the CNT on SiO_2 samples. There is a peak referring to SiC. **d** Raman spectra present an SiC peak. **f** An SiC particle encapsulates inside the CNT tip. (**e**–**h**) HRTEM of the CNT with a cap tip or with opening tip. Schematic showing reduction of SiO2 catalyst particle to SiC and subsequent carbon tube/fiber growth (**i**). Reprinted (adapted) with permission from Ref [281]. Copyright (2009) American Chemical Society

Acknowledgements J.P. thanks the China Scholarship Council (CSC) and the DFG (DFG RU1540/15-2). A.B. thanks the National Science Centre for the financial support within the frames of the Sonata Programme (Grant agreement 2014/13/D/ST5/02853). D.P. and G.S.M. thank the IT4 Innovations project reg. no. CZ.1.05./1.1.00/02.0070. The research was supported by the Sino-German Center for Research Promotion (Grant GZ 871). J.E. thanks the German Excellence Initiative via the Cluster of Excellence EXC1056 "Center for Advancing Electronics Dresden" (CfAED).

Authors' contributions The manuscript was written through contributions of all authors.

Compliance with ethical standards

Conflict of interest The authors declare that they have no competing interests.

References

1. Warner JH, Schäffel F, Bachmatiuk A, Rümmeli MH (2013) Graphene fundamentals and emergent applications, 1st edn. Elsevier, Waltham
2. Rummeli MH, Ayala P, Pichler T (2010) Carbon nanotubes and related structures: production and formation. In: Guldi DM, Martín N (eds) Carbon nanotub. Relat. Struct. Wiley-VCH Verlag GmbH & Co, KGaA, Weinheim, Germany, pp 1–21
3. Liu Z, Liu JZ, Cheng Y et al (2012) Interlayer binding energy of graphite: a mesoscopic determination from deformation. Phys Rev B 85:205418
4. Rümmeli MH, Rocha CG, Ortmann F et al (2011) Graphene: piecing it together. Adv Mater 23:4471–4490
5. Fallahazad B, Hao Y, Lee K et al (2012) Quantum Hall effect in Bernal stacked and twisted bilayer graphene grown on Cu by chemical vapor deposition. Phys Rev B 85:1–5
6. Novoselov KS, Jiang Z, Zhang Y et al (2007) Room-temperature quantum Hall effect in graphene. Science 315:1379
7. Han P, Akagi K, Canova FF et al (2014) Bottom-up graphene-nanoribbon fabrication reveals chiral edges and enantioselectivity. ACS Nano 8:9181–9187
8. Sangwan VK, Jariwala D, Everaerts K et al (2014) Wafer-scale solution-derived molecular gate dielectrics for low-voltage graphene electronics. Appl Phys Lett 104:083503
9. Ang PK, Li A, Jaiswal M et al (2011) Flow sensing of single cell by graphene transistor in a microfluidic channel. Nano Lett 11:5240–5246
10. Yan Z, Peng Z, Sun Z et al (2011) Growth of bilayer graphene on insulating substrates. ACS Nano 5:8187–8192
11. Liu L, Zhou H, Cheng R et al (2012) High-yield chemical vapor deposition growth of high-quality large-area AB-stacked bilayer graphene. ACS Nano 6:8241–8249
12. Wu Y, Chou H, Ji H et al (2012) Growth mechanism and controlled synthesis of AB-stacked bilayer graphene on Cu-Ni alloy foils. ACS Nano 6:7731–7738
13. Yan K, Peng H, Zhou Y et al (2011) Formation of bilayer bernal graphene: Layer-by-layer epitaxy via chemical vapor deposition. Nano Lett 11:1106–1110
14. Xia F, Farmer DB, Lin YM, Avouris P (2010) Graphene field-effect transistors with high on/off current ratio and large transport band gap at room temperature. Nano Lett 10:715–718

15. Yu WJ, Liao L, Chae SH et al (2011) Toward tunable band gap and tunable dirac point in bilayer graphene with molecular doping. Nano Lett 11:4759–4763
16. Bachmatiuk A, Mendes RG, Hirsch C et al (2013) Few-layer graphene shells and nonmagnetic encapsulates: a versatile and nontoxic carbon nanomaterial. ACS Nano 7:10552–10562
17. Deng J, Chen L, Sun Y et al (2015) Interconnected MnO_2 nanoflakes assembled on graphene foam as a binder-free and long-cycle life lithium battery anode. Carbon 92:177–184
18. Guo J, Zhang T, Hu C, Fu L (2015) A three-dimensional nitrogen-doped graphene structure: a highly efficient carrier of enzymes for biosensors. Nanoscale 7:1290–1295
19. Hu X, Ma M, Zeng M et al (2014) Supercritical carbon dioxide anchored Fe_3O_4 nanoparticles on graphene foam and lithium battery performance. ACS Appl Mater Interfaces 6:22527–22533
20. Liu J, Leng X, Xiao Y et al (2015) 3D nitrogen-doped graphene/β-cyclodextrin: host–guest interactions for electrochemical sensing. Nanoscale 7:11922–11927
21. Bachmatiuk A, Boeckl J, Smith H et al (2015) Vertical graphene growth from amorphous carbon films using oxidizing gases. J Phys Chem C 119:17965–17970
22. Davami K, Shaygan M, Kheirabi N et al (2014) Synthesis and characterization of carbon nanowalls on different substrates by radio frequency plasma enhanced chemical vapor deposition. Carbon 72:372–380
23. Zhao J, Shaygan M, Eckert J et al (2014) A growth mechanism for free-standing vertical graphene. Nano Lett 14:3064–3071
24. Park H, Chang S, Jean J et al (2013) Graphene cathode-based ZnO nanowire hybrid solar cells. Nano Lett 13:233–239
25. Chattopadhyay S, Lipson AL, Karmel HJ et al (2012) In situ X-ray study of the solid electrolyte interphase (SEI) formation on graphene as a model Li-ion battery anode. Chem Mater 24:3038–3043
26. Cheng Y, Lu S, Zhang H et al (2012) Synergistic effects from graphene and carbon nanotubes enable flexible and robust electrodes for high-performance supercapacitors. Nano Lett 12:4206–4211
27. Liang YT, Vijayan BK, Gray KA, Hersam MC (2011) Minimizing graphene defects enhances titania nanocomposite-based photocatalytic reduction of CO_2 for improved solar fuel production. Nano Lett 11:2865–2870
28. Lu S, Cheng Y, Wu X, Liu J (2013) Significantly improved long-cycle stability in high-rate Li-S batteries enabled by coaxial graphene wrapping over sulfur-coated carbon nanofibers. Nano Lett 13:2485–2489
29. Ma Y, Li P, Sedloff JW et al (2015) conductive graphene fibers for wire-shaped supercapacitors strengthened by unfunctionalized few-walled carbon nanotubes. ACS Nano 9:1352–1359
30. Wang Y, Tong SW, Xu XF et al (2011) Interface engineering of layer-by-layer stacked graphene anodes for high-performance organic solar cells. Adv Mater 23:1514–1518
31. Yusoff ARBM, Dai L, Cheng H-M, Liu J (2015) Graphene based energy devices. Nanoscale 7:6881–6882
32. Zang J, Cao C, Feng Y et al (2014) Stretchable and high-performance supercapacitors with crumpled graphene papers. Sci Rep 4:6492
33. Lee C, Wei X, Kysar JW, Hone J (2008) Measurement of the elastic properties and intrinsic strength of monolayer graphene. Science 321:385–388
34. Zhao H, Min K, Aluru NR (2009) Size and chirality dependent elastic properties of graphene nanoribbons under uniaxial tension. Nano Lett 9:3012–3015
35. Kalaitzidou K, Fukushima H, Askeland P, Drzal LT (2008) The nucleating effect of exfoliated graphite nanoplatelets and their influence on the crystal structure and electrical conductivity of polypropylene nanocomposites. J Mater Sci 43:2895–2907
36. Bao Q, Zhang H, Wang B et al (2011) Broadband graphene polarizer. Nat Photonics 5:411–415
37. Nair RR, Blake P, Grigorenko AN et al (2008) Fine structure constant defines visual transparency of graphene. Science 320:1308
38. Huang PY, Ruiz-Vargas CS, van der Zande AM et al (2011) Grains and grain boundaries in single-layer graphene atomic patchwork quilts. Nature 469:389–392
39. Kim K, Lee Z, Regan W et al (2011) Grain boundary mapping in polycrystalline graphene. ACS Nano 5:2142–2146
40. Liu Z, Suenaga K, Harris PJF, Iijima S (2009) Open and closed edges of graphene layers. Phys Rev Lett 102:015501
41. Hashimoto A, Suenaga K, Gloter A et al (2004) Direct evidence for atomic defects in graphene layers. Nature 430:870–873
42. Meyer JC, Kisielowski C, Erni R et al (2008) Direct imaging of lattice atoms and topological defects in graphene membranes. Nano Lett 8:3582–3586
43. Cortijo A, Vozmediano MAH (2007) Electronic properties of curved graphene sheets. Europhys Lett 77:47002
44. Cortijo A, Vozmediano MAH (2007) Effects of topological defects and local curvature on the electronic properties of planar graphene. Nucl Phys B 763:293–308
45. Banhart F, Kotakoski J, Krasheninnikov AV (2011) Structural defects in graphene. ACS Nano 5:26–41
46. Warner JH, Margine ER, Mukai M et al (2012) Dislocation-driven deformations in graphene. Science 337:209–212
47. Bao Q, Zhang H, Yang J et al (2010) Graphene-polymer nanofiber membrane for ultrafast photonics. Adv Funct Mater 20:782–791
48. Hossain MZ, Johns JE, Bevan KH et al (2012) Chemically homogeneous and thermally reversible oxidation of epitaxial graphene. Nat Chem 4:305–309
49. Hossain MZ, Walsh MA, Hersam MC (2010) Scanning tunneling microscopy, spectroscopy, and nanolithography of epitaxial graphene chemically modified with aryl moieties. J Am Chem Soc 132:15399–15403
50. Manga KK, Wang S, Jaiswal M et al (2010) High-gain graphene-titanium oxide photoconductor made from inkjet printable ionic solution. Adv Mater 22:5265–5270
51. Mendes RG, Koch B, Bachmatiuk A et al (2015) A size dependent evaluation of the cytotoxicity and uptake of nano-graphene oxide. J Mater Chem B 3:2522–2529
52. Yan L, Zheng YB, Zhao F et al (2012) Chemistry and physics of a single atomic layer: strategies and challenges for functionalization of graphene and graphene-based materials. Chem Soc Rev 41:97–114
53. Johns JE, Hersam MC (2013) Atomic covalent functionalization of graphene. Acc Chem Res 46:77–86
54. Mendes RG, Bachmatiuk A, Büchner B et al (2013) Carbon nanostructures as multi-functional drug delivery platforms. J Mater Chem B 1:401–428
55. Choi Gill B, Park Jung T, Yang Ho M et al (2010) Solution chemistry of self-assembled graphene nanohybrids for high-performance flexible biosensors. ACS Nano 4:2910–2918
56. Bi H, Yin K, Xie X et al (2013) Ultrahigh humidity sensitivity of graphene oxide. Sci Rep 3:2714
57. Liu S, Zeng TH, Hofmann M et al (2011) Antibacterial activity of graphite, graphite oxide, graphene oxide, and reduced graphene oxide: membrane and oxidative stress. ACS Nano 5:6971–6980
58. Wang H, Cui L-F, Yang Y et al (2010) Mn_3O_4—graphene hybrid as a high-capacity anode material for lithium ion batteries. J Am Chem Soc 132:13978–13980

59. Li Y, Wang H, Xie L et al (2011) MoS_2 nanoparticles grown on graphene: an advanced catalyst for the hydrogen evolution reaction. J Am Chem Soc 133:7296–7299
60. Dresselhaus MS, Jorio A, Saito R (2010) Characterizing graphene, graphite, and carbon nanotubes by raman spectroscopy. Annu Rev Condens Matter Phys 1:89–108
61. Benedict LX, Crespi VH, Louie SG, Cohen ML (1995) Static conductivity and superconductivity of carbon nanotubes: relations between tubes and sheets. Phys Rev B 52:14935–14940
62. Kim W, Choi HC, Shim M et al (2002) Synthesis of ultralong and high percentage of semiconducting single-walled carbon nanotubes. Nano Lett 2:703–708
63. Odom TW, Huang J-L, Kim P, Lieber CM (2000) Structure and electronic properties of carbon nanotubes. J Phys Chem B 104:2794–2809
64. Popov VN, Lambin P (2006) Radius and chirality dependence of the radial breathing mode and the G-band phonon modes of single-walled carbon nanotubes. Phys Rev B 73:085407
65. Sasaki K-I, Saito R, Dresselhaus G et al (2008) Curvature-induced optical phonon frequency shift in metallic carbon nanotubes. Phys Rev B 77:245441
66. Jiang J, Saito R, Samsonidze GG et al (2007) Chirality dependence of exciton effects in single-wall carbon nanotubes: tight-binding model. Phys Rev B 75:035407
67. Popov VN (2004) Curvature effects on the structural, electronic and optical properties of isolated single-walled carbon nanotubes within a symmetry-adapted non-orthogonal tight-binding model. New J Phys 6:17
68. Dresselhaus MS, Dresselhaus G, Charlier JC, Hernandez E (2004) Electronic, thermal and mechanical properties of carbon nanotubes. Philos Trans R Soc A Math Phys Eng Sci 362:2065–2098
69. Dresselhaus MS, Dresselhaus G, Jorio A (2004) Unusual properties and structure of carbon nanotubes. Annu Rev Mater Res 34:247–278
70. Krasheninnikov AV, Banhart F, Li JX et al (2005) Stability of carbon nanotubes under electron irradiation: role of tube diameter and chirality. Phys Rev B 72:125428
71. Sun G, Kürti J, Kertesz M, Baughman RH (2003) Variations of the geometries and band gaps of single-walled carbon nanotubes and the effect of charge injection. J Phys Chem B 107:6924–6931
72. Anantram MP, Léonard F (2006) Physics of carbon nanotube electronic devices. Reports Prog Phys 69:507–561
73. Blase X, Benedict LX, Shirley EL, Louie SG (1994) Hybridization effects and metallicity in small radius carbon nanotubes. Phys Rev Lett 72:1878–1881
74. Stéphan O, Ajayan PM, Colliex C et al (1996) Curvature-induced bonding changes in carbon nanotubes investigated by electron energy-loss spectrometry. Phys Rev B 53:13824–13829
75. Cabria I, Mintmire JW, White CT (2003) Metallic and semiconducting narrow carbon nanotubes. Phys Rev B 67:121406
76. Hasan T, Sun Z, Tan P et al (2014) Double-wall carbon nanotubes for wide-band, ultrafast pulse generation. ACS Nano 8:4836–4847
77. Zhang R, Ning Z, Zhang Y et al (2013) Superlubricity in centimetres-long double-walled carbon nanotubes under ambient conditions. Nat Nanotechnol 8:912–916
78. Rümmeli MH, Schäffel F, Bachmatiuk A et al (2010) Investigating the outskirts of Fe and Co catalyst particles in alumina-supported catalytic CVD carbon nanotube growth. ACS Nano 4:1146–1152
79. Iijima S (1991) Helical microtubules of graphitic carbon. Nature 354:56–58
80. Rümmeli MH, Schäffel F, Kramberger C et al (2007) Oxide-driven carbon nanotube growth in supported catalyst CVD. J Am Chem Soc 129:15772–15773
81. Borowiak-Palen E, Rümmeli MH (2009) Activated Cu catalysts for alcohol CVD synthesized non-magnetic bamboo-like carbon nanotubes and branched bamboo-like carbon nanotubes. Superlattices Microstruct 46:374–378
82. Lin M, Tan JPY, Boothroyd C et al (2007) Dynamical observation of bamboo-like carbon nanotube growth. Nano Lett 7:2234–2238
83. Hofmann S, Sharma R, Ducati C et al (2007) In situ observations of catalyst dynamics during surface-bound carbon nanotube nucleation. Nano Lett 7:602–608
84. Ouyang M, Huang J-L, Lieber CM (2002) Fundamental electronic properties and applications of single-walled carbon nanotubes. Acc Chem Res 35:1018–1025
85. Green AA, Hersam MC (2008) Colored semitransparent conductive coatings consisting of monodisperse metallic single-walled carbon nanotubes. Nano Lett 8:1417–1422
86. Lieber CM, Odom TW, Huang J-L, Kim P (1998) Atomic structure and electronic properties of single-walled carbon nanotubes. Nature 391:62–64
87. Sangwan VK, Ortiz RP, Alaboson JMP et al (2012) Fundamental performance limits of carbon nanotube thin-film transistors achieved using hybrid molecular dielectrics. ACS Nano 6:7480–7488
88. Wang H, Luo J, Robertson A et al (2010) High-performance field effect transistors from solution processed carbon nanotubes. ACS Nano 4:6659–6664
89. Rueckes T, Kim K, Joselevich E et al (2000) Carbon nanotube-based nonvolatile random access memory for molecular computing. Science 289:94–97
90. Amade R, Vila-Costa M, Hussain S et al (2015) Vertically aligned carbon nanotubes coated with manganese dioxide as cathode material for microbial fuel cells. J Mater Sci 50:1214–1220
91. Abbas SM, Hussain ST, Ali S et al (2013) Structure and electrochemical performance of ZnO/CNT composite as anode material for lithium-ion batteries. J Mater Sci 48:5429–5436
92. Deng Q, Wang L, Li J (2015) Electrochemical characterization of Co_3O_4/MCNTs composite anode materials for sodium-ion batteries. J Mater Sci 50:4142–4148
93. Fam DWH, Azoubel S, Liu L et al (2015) Novel felt pseudocapacitor based on carbon nanotube/metal oxides. J Mater Sci 50:6578–6585
94. Hussain S, Amade R, Jover E, Bertran E (2013) Nitrogen plasma functionalization of carbon nanotubes for supercapacitor applications. J Mater Sci 48:7620–7628
95. Byrappa K, Dayananda AS, Sajan CP et al (2008) Hydrothermal preparation of ZnO:CNT and TiO_2:CNT composites and their photocatalytic applications. J Mater Sci 43:2348–2355
96. Hu G, Meng X, Feng X et al (2007) Anatase TiO_2 nanoparticles/carbon nanotubes nanofibers: preparation, characterization and photocatalytic properties. J Mater Sci 42:7162–7170
97. Li X, Wei J, Chai Y et al (2015) Different polyaniline/carbon nanotube composites as Pt catalyst supports for methanol electro-oxidation. J Mater Sci 50:1159–1168
98. Dresselhaus MS, Dresselhaus G, Avouris P (2001) Carbon nanotubes synthesis, structure, properties, and applications. Springer, Berlin
99. Louie SG (2001) Electronic properties, junctions, and defects of carbon nanotubes. Carbon Nanotub. Springer, Berlin, pp 113–145
100. Saito R, Dresselhaus G, Dresselhaus MS (1998) Physical properties of carbon nanotubes. Imperial College Press, London

101. Young PN, Kirkland IA, Briggs Andrew DG et al (2011) Resolving strain in carbon nanotubes at the atomic level. Nat Mater 10:958–962
102. Dresselhaus MS, Avouris P Introduction to Carbon Materials Research. In: Carbon Nanotub. Springer Berlin Heidelberg, Heidelberg, pp 1–9
103. Crespi VH, Cohen ML, Rubio A (1997) In situ band gap engineering of carbon nanotubes. Phys Rev Lett 79:2093–2096
104. Odom TW, Hafner JH, Lieber CM (2001) Scanning probe microscopy studies of carbon nanotubes. Carbon Nanotub. Springer, Berlin, pp 173–211
105. Ouyang M, Huang J-L, Cheung CL, Lieber CM (2001) Energy gaps in "metallic" single-walled carbon nanotubes. Science 292:702–705
106. Zhou C, Kong J, Dai H (2000) Intrinsic electrical properties of individual single-walled carbon nanotubes with small band gaps. Phys Rev Lett 84:5604–5607
107. Hamada N, Sawada S, Oshiyama A (1992) New one-dimensional conductors: graphitic microtubules. Phys Rev Lett 68:1579–1581
108. Kane CL, Mele EJ (1997) Size, shape, and low energy electronic structure of carbon nanotubes. Phys Rev Lett 78:1932–1935
109. Mintmire JW, White CT (1995) Electronic and structural properties of carbon nanotubes. Carbon 33:893–902
110. Ding JW, Yan XH, Cao JX (2002) Analytical relation of band gaps to both chirality and diameter of single-wall carbon nanotubes. Phys Rev B 66:073401
111. Dresselhaus MS, Dresselhaus G, Saito R (1992) C60-related tubules. Solid State Commun 84:201–205
112. White CT, Robertson DH, Mintmire JW (1993) Helical and rotational symmetries of nanoscale graphitic tubules. Phys Rev B 47:5485–5488
113. Hayashi T, Kim YA, Matoba T et al (2003) Smallest freestanding single-walled carbon nanotube. Nano Lett 3:887–889
114. Weisman RB, Bachilo SM (2003) Dependence of optical transition energies on structure for single-walled carbon nanotubes in aqueous suspension: an empirical Kataura plot. Nano Lett 3:1235–1238
115. O'Connell MJ, Bachilo SM, Huffman CB et al (2002) Band gap fluorescence from individual single-walled carbon nanotubes. Science 297:593–596
116. Arnold MS, Green AA, Hulvat JF et al (2006) Sorting carbon nanotubes by electronic structure using density differentiation. Nat Nanotechnol 1:60–65
117. Ebbesen TW, Takada T (1995) Topological and SP3 defect structures in nanotubes. Carbon 33:973–978
118. Lambin P, Fonseca A, Vigneron JP et al (1995) Structural and electronic properties of bent carbon nanotubes. Chem Phys Lett 245:85–89
119. Saito R, Dresselhaus G, Dresselhaus MS (1996) Tunneling conductance of connected carbon nanotubes. Phys Rev B 53:2044–2050
120. Dunlap BI (1994) Relating carbon tubules. Phys Rev B 49:5643–5651
121. Charlier J-C, Ebbesen TW, Lambin P (1996) Structural and electronic properties of pentagon-heptagon pair defects in carbon nanotubes. Phys Rev B 53:11108–11113
122. Chico L, Crespi VH, Benedict LX et al (1996) Pure carbon nanoscale devices: nanotube heterojunctions. Phys Rev Lett 76:971–974
123. Chico L, Benedict LX, Louie SG, Cohen ML (1996) Quantum conductance of carbon nanotubes with defects. Phys Rev B 54:2600–2606
124. Wang B, Yanfeng M, Li N et al (2010) Facile and scalable fabrication of well-aligned and closely packed single-walled carbon nanotube films on various substrates. Adv Mater 22:3067–3070
125. Wong EW, Sheehan PE, Lieber CM (1997) Nanobeam mechanics: elasticity, strength, and toughness of nanorods and nanotubes. Science 277:1971–1975
126. Dufresne A, Paillet M, Putaux JL et al (2002) Processing and characterization of carbon nanotube/poly(styrene-co-butyl acrylate) nanocomposites. J Mater Sci 37:3915–3923
127. Hsieh TH, Kinloch AJ, Taylor AC, Kinloch IA (2011) The effect of carbon nanotubes on the fracture toughness and fatigue performance of a thermosetting epoxy polymer. J Mater Sci 46:7525–7535
128. Suhr J, Koratkar NA (2008) Energy dissipation in carbon nanotube composites: a review. J Mater Sci 43:4370–4382
129. Bozovic D, Bockrath M, Hafner JH et al (2003) Plastic deformations in mechanically strained single-walled carbon nanotubes. Phys Rev B 67:033407
130. Dieringa H (2011) Properties of magnesium alloys reinforced with nanoparticles and carbon nanotubes: a review. J Mater Sci 46:289–306
131. Cho J, Boccaccini AR, Shaffer MSP (2009) Ceramic matrix composites containing carbon nanotubes. J Mater Sci 44:1934–1951
132. Kathi J, Rhee KY (2008) Surface modification of multi-walled carbon nanotubes using 3-aminopropyltriethoxysilane. J Mater Sci 43:33–37
133. Chen L, Chin LC, Ashby PD, Lieber CM (2004) Single-walled carbon nanotube AFM probes: optimal imaging resolution of nanoclusters and biomolecules in ambient and fluid environments. Nano Lett 4:1725–1731
134. Kim P, Lieber CM (1999) Nanotube nanotweezers. Science 286:2148–2150
135. Kim P, Shi L, Majumdar A, McEuen PL (2001) Thermal transport measurements of individual multiwalled nanotubes. Phys Rev Lett 87:215502
136. Yao Z, Wang J-S, Li B, Liu G-R (2005) Thermal conduction of carbon nanotubes using molecular dynamics. Phys Rev B 71:085417
137. Iijima S (2002) Carbon nanotubes: past, present, and future. Phys B Condens Matter 323:1–5
138. Bajpai A, Gorantla S, Löffler M et al (2012) The filling of carbon nanotubes with magnetoelectric Cr2O3. Carbon 50:1706–1709
139. Cichocka MO, Zhao J, Bachmatiuk A et al (2014) In situ observations of Pt nanoparticles coalescing inside carbon nanotubes. RSC Adv 4:49442–49445
140. Gorantla S, Börrnert F, Bachmatiuk A et al (2010) In situ observations of fullerene fusion and ejection in carbon nanotubes. Nanoscale 2:2077
141. Pohl D, Schäffel F, Rümmeli MH et al (2011) Understanding the metal-carbon interface in FePt catalyzed carbon nanotubes. Phys Rev Lett 107:185501
142. Dillon AC, Jones KM, Bekkedahl TA et al (1997) Storage of hydrogen in single-walled carbon nanotubes. Nature 386:377–379
143. Liu C, Chen Y, Wu C-Z et al (2010) Hydrogen storage in carbon nanotubes revisited. Carbon 48:452–455
144. Schlapbach L, Züttel A (2001) Hydrogen-storage materials for mobile applications. Nature 414:353–358
145. Wang Q, Johnson JK (1999) Molecular simulation of hydrogen adsorption in single-walled carbon nanotubes and idealized carbon slit pores. J Chem Phys 110:577
146. Byl O, Kondratyuk P, Yates JT (2003) Adsorption and dimerization of NO inside single-walled carbon nanotubes an infrared spectroscopic study. J Phys Chem B 107:4277–4279

147. Fujiwara A, Ishii K, Suematsu H et al (2001) Gas adsorption in the inside and outside of single-walled carbon nanotubes. Chem Phys Lett 336:205–211
148. Kuznetsova A, Yates JT, Liu J, Smalley RE (2000) Physical adsorption of xenon in open single walled carbon nanotubes: observation of a quasi-one-dimensional confined Xe phase. J Chem Phys 112:9590
149. Shiomi J, Maruyama S (2009) Water transport inside a single-walled carbon nanotube driven by a temperature gradient. Nanotechnology 20:055708
150. Noy A, Park HG, Fornasiero F et al (2007) Nanofluidics in carbon nanotubes. Nano Today 2:22–29
151. Maniwa Y, Matsuda K, Kyakuno H et al (2007) Water-filled single-wall carbon nanotubes as molecular nanovalves. Nat Mater 6:135–141
152. Zhao Y, Song L, Deng K et al (2008) Individual water-filled single-walled carbon nanotubes as hydroelectric power converters. Adv Mater 20:1772–1776
153. Maniwa Y, Kataura H, Abe M et al (2005) Ordered water inside carbon nanotubes: formation of pentagonal to octagonal ice-nanotubes. Chem Phys Lett 401:534–538
154. Koga K, Gao GT, Tanaka H, Zeng XC (2001) Formation of ordered ice nanotubes inside carbon nanotubes. Nature 412:802–805
155. Pan X, Fan Z, Chen W et al (2007) Enhanced ethanol production inside carbon-nanotube reactors containing catalytic particles. Nat Mater 6:507–511
156. Tessonnier J-P, Pesant L, Ehret G et al (2005) Pd nanoparticles introduced inside multi-walled carbon nanotubes for selective hydrogenation of cinnamaldehyde into hydrocinnamaldehyde. Appl Catal A Gen 288:203–210
157. Yoshitake T, Shimakawa Y, Kuroshima S et al (2002) Preparation of fine platinum catalyst supported on single-wall carbon nanohorns for fuel cell application. Phys B Condens Matter 323:124–126
158. Shiozawa H, Pichler T, Grüneis A et al (2008) A catalytic reaction inside a single-walled carbon nanotube. Adv Mater 20:1443–1449
159. Pan X, Bao X (2011) The effects of confinement inside carbon nanotubes on catalysis. Acc Chem Res 44:553–562
160. Chen W, Fan Z, Gu L et al (2010) Enhanced capacitance of manganese oxide via confinement inside carbon nanotubes. Chem Commun 46:3905
161. Yang C-K, Zhao J, Lu JP (2003) Magnetism of transition-metal/carbon-nanotube hybrid structures. Phys Rev Lett 90:257203
162. Hirahara K, Suenaga K, Bandow S et al (2000) One-dimensional metallofullerene crystal generated inside single-walled carbon nanotubes. Phys Rev Lett 85:5384–5387
163. Gao H, Kong Y, Cui D, Ozkan CS (2003) Spontaneous insertion of DNA oligonucleotides into carbon nanotubes. Nano Lett 3:471–473
164. Liu Z, Yanagi K, Suenaga K et al (2007) Imaging the dynamic behaviour of individual retinal chromophores confined inside carbon nanotubes. Nat Nanotechnol 2:422–425
165. Kong J, Chapline MG, Dai H (2001) Functionalized carbon nanotubes for molecular hydrogen sensors. Adv Mater 13:1384–1386
166. Chen RJ, Zhang Y, Wang D, Dai H (2001) Noncovalent sidewall functionalization of single-walled carbon nanotubes for protein immobilization. J Am Chem Soc 123:3838–3839
167. Chen RJ, Bangsaruntip S, Drouvalakis KA et al (2003) Noncovalent functionalization of carbon nanotubes for highly specific electronic biosensors. Proc Natl Acad Sci 100:4984–4989
168. Lieber CM, Wong SS, Joselevich E et al (1998) Covalently functionalized nanotubes as nanometre- sized probes in chemistry and biology. Nature 394:52–55
169. Hain TC, Kröker K, Stich DG, Hertel T (2012) Influence of DNA conformation on the dispersion of SWNTs: single-strand DNA versus hairpin DNA. Soft Matter 8:2820
170. Sun H, She P, Lu G et al (2014) Recent advances in the development of functionalized carbon nanotubes: a versatile vector for drug delivery. J Mater Sci 49:6845–6854
171. Ayala P, Plank W, Grüneis A et al (2008) A one step approach to B-doped single-walled carbon nanotubes. J Mater Chem 18:5676–5681
172. Gong K, Du F, Xia Z et al (2009) Nitrogen-doped carbon nanotube arrays with high electrocatalytic activity for oxygen reduction. Science 323:760–764
173. Yu D, Zhang Q, Dai L (2010) Highly efficient metal-free growth of nitrogen-doped single-walled carbon nanotubes on plasma-etched substrates for oxygen reduction. J Am Chem Soc 132:15127–15129
174. Chopra NG, Luyken RJ, Cherrey K et al (1995) Boron nitride nanotubes. Science 269:966–967
175. Gonzalez-Martinez IG, Gorantla SM, Bachmatiuk A et al (2014) Room temperature in situ growth of B/BOx nanowires and BOx nanotubes. Nano Lett 14:799–805
176. Lourie OR, Jones CR, Bartlett BM et al (2000) CVD growth of boron nitride nanotubes. Chem Mater 12:1808–1810
177. Novoselov KS, Geim AK, Morozov SV et al (2004) Electric field effect in atomically thin carbon films. Science 306:666–669
178. Makharza S, Cirillo G, Bachmatiuk A et al (2013) Graphene oxide-based drug delivery vehicles: functionalization, characterization, and cytotoxicity evaluation. J Nanoparticle Res 15:2099
179. Stankovich S, Dikin AD, Piner DR et al (2007) Synthesis of graphene-based nanosheets via chemical reduction of exfoliated graphite oxide. Carbon 45:1558–1565
180. Tamboli SH, Kim BS, Choi G et al (2014) Post-heating effects on the physical and electrochemical capacitive properties of reduced graphene oxide paper. J Mater Chem A 2:5077
181. Liang YT, Hersam MC (2010) Highly concentrated graphene solutions via polymer enhanced solvent exfoliation and iterative solvent exchange. J Am Chem Soc 132:17661–17663
182. Wang J, Manga KK, Bao Q, Loh KP (2011) High-yield synthesis of few-layer graphene flakes through electrochemical expansion of graphite in propylene carbonate electrolyte. J Am Chem Soc 133:8888–8891
183. Jiao L, Zhang L, Ding L et al (2010) Aligned graphene nanoribbons and crossbars from unzipped carbon nanotubes. Nano Res 3:387–394
184. Li X, Wang X, Zhang L et al (2008) Chemically derived, ultrasmooth graphene nanoribbon semiconductors. Science 319:1229–1232
185. Cai J, Ruffieux P, Jaafar R et al (2010) Atomically precise bottom-up fabrication of graphene nanoribbons. Nature 466:470–473
186. Emtsev KV, Speck F, Seyller T et al (2008) Interaction, growth, and ordering of epitaxial graphene on SiC{0001} surfaces: a comparative photoelectron spectroscopy study. Phys Rev B 77:155303
187. Emtsev KV, Bostwick A, Horn K et al (2009) Towards wafer-size graphene layers by atmospheric pressure graphitization of silicon carbide. Nat Mater 8:203–207
188. Dai B, Fu L, Zou Z et al (2011) Rational design of a binary metal alloy for chemical vapour deposition growth of uniform single-layer graphene. Nat Commun 2:522

189. Liu X, Fu L, Liu N et al (2011) Segregation growth of graphene on Cu-Ni alloy for precise layer control. J Phys Chem C 115:11976–11982
190. Rümmeli MH, Zeng M, Melkhanova S et al (2013) Insights into the early growth of homogeneous single-layer graphene over Ni-Mo binary substrates. Chem Mater 25:3880–3887
191. Zou Z, Fu L, Song X et al (2014) Carbide-forming groups IVB-VIB metals: a new territory in the periodic table for CVD growth of graphene. Nano Lett 14:3832–3839
192. Pang J, Bachmatiuk A, Fu L et al (2015) Direct synthesis of graphene from adsorbed organic solvent molecules over copper. RSC Adv 5:60884–60891
193. Mendes RG, Bachmatiuk A, El-Gendy AA et al (2012) A Facile route to coat iron oxide nanoparticles with few-layer graphene. J Phys Chem C 116:23749–23756
194. Li X, Cai W, An J et al (2009) Large-area synthesis of high-quality and uniform graphene films on copper foils. Science 324:1312–1314
195. Pang J, Bachmatiuk A, Fu L et al (2015) Oxidation as a means to remove surface contaminants on Cu foil prior to graphene growth by chemical vapor deposition. J Phys Chem C 119:13363–13368
196. Rümmeli MH, Gorantla S, Bachmatiuk A et al (2013) On the role of vapor trapping for chemical vapor deposition (CVD) grown graphene over copper. Chem Mater 25:4861–4866
197. Riikonen J, Kim W, Li C et al (2013) Photo-thermal chemical vapor deposition of graphene on copper. Carbon 62:43–50
198. Kim SM, Hsu A, Lee Y et al (2013) The effect of copper pre-cleaning on graphene synthesis. Nanotechnology 24:365602
199. Hao Y, Bharathi MS, Wang L et al (2013) The role of surface oxygen in the growth of large single-crystal graphene on copper. Science 342:720–723
200. Luo Z, Lu Y, Singer DW et al (2011) Effect of substrate roughness and feedstock concentration on growth of wafer-scale graphene at atmospheric pressure. Chem Mater 23:1441–1447
201. Procházka P, Mach J, Bischoff D et al (2014) Ultrasmooth metallic foils for growth of high quality graphene by chemical vapor deposition. Nanotechnology 25:185601
202. Eres G, Regmi M, Rouleau CM et al (2014) Cooperative island growth of large-area single-crystal graphene on copper using chemical vapor deposition. ACS Nano 8:5657–5669
203. Tan L, Zeng M, Zhang T, Fu L (2015) Design of catalytic substrates for uniform graphene films: from solid-metal to liquid-metal. Nanoscale 7:9105–9121
204. Zeng M, Tan L, Wang J et al (2014) Liquid metal: an innovative solution to uniform graphene films. Chem Mater 26:3637–3643
205. Magnuson CW, Kong X, Ji H et al (2014) Copper oxide as a "self-cleaning" substrate for graphene growth. J Mater Res 29:403–409
206. Vlassiouk I, Regmi M, Fulvio P et al (2011) Role of hydrogen in chemical vapor deposition growth of large single-crystal graphene. ACS Nano 5:6069–6076
207. Han GH, Güneş F, Bae JJ et al (2011) Influence of copper morphology in forming nucleation seeds for graphene growth. Nano Lett 11:4144–4148
208. Kim KSKS, Zhao Y, Jang H et al (2009) Large-scale pattern growth of graphene films for stretchable transparent electrodes. Nature 457:706–710
209. Tan L, Zeng M, Wu Q et al (2015) Direct growth of ultrafast transparent single-layer graphene defoggers. Small 11:1840–1846
210. Chen J, Wen Y, Guo Y et al (2011) Oxygen-aided synthesis of polycrystalline graphene on silicon dioxide substrates. J Am Chem Soc 133:17548–17551
211. Sutter P, Hybertsen MS, Sadowski JT, Sutter E (2009) Electronic structure of few-layer epitaxial graphene on Ru(0001). Nano Lett 9:2654–2660
212. Ramón ME, Gupta A, Corbet C et al (2011) CMOS-compatible synthesis of large-area, high-mobility graphene by chemical vapor deposition of acetylene on cobalt thin films. ACS Nano 5:7198–7204
213. An H, Lee W-J, Jung J (2011) Graphene synthesis on Fe foil using thermal CVD. Curr Appl Phys 11:S81–S85
214. John R, Ashokreddy A, Vijayan C, Pradeep T (2011) Single- and few-layer graphene growth on stainless steel substrates by direct thermal chemical vapor deposition. Nanotechnology 22:165701
215. Kiraly B, Iski EV, Mannix AJ et al (2013) Solid-source growth and atomic-scale characterization of graphene on Ag(111). Nat Commun 4:2804
216. Reina A, Jia X, Ho J et al (2009) Large area, few-layer graphene films on arbitrary substrates by chemical vapor deposition. Nano Lett 9:30–35
217. Reina A, Thiele S, Jia X et al (2009) Growth of large-area single- and Bi-layer graphene by controlled carbon precipitation on polycrystalline Ni surfaces. Nano Res 2:509–516
218. Li X, Cai W, Colombo L et al (2009) Evolution of graphene growth on Ni and Cu by carbon isotope labeling. Nano Lett 9:4268–4272
219. Bae S, Kim H, Lee Y et al (2010) Roll-to-roll production of 30-inch graphene films for transparent electrodes. Nat Nanotechnol 5:574–578
220. Tao L, Lee J, Chou H et al (2012) Synthesis of high quality monolayer graphene at reduced temperature on hydrogen-enriched evaporated copper (111) films. ACS Nano 6:2319–2325
221. Ismach A, Druzgalski C, Penwell S et al (2010) Direct chemical vapor deposition of graphene on dielectric surfaces. Nano Lett 10:1542–1548
222. Chen J, Guo Y, Jiang L et al (2014) Near-equilibrium chemical vapor deposition of high-quality single-crystal graphene directly on various dielectric substrates. Adv Mater 26:1348–1353
223. Hwang J, Kim M, Campbell D et al (2013) Van der waals epitaxial growth of graphene on sapphire by chemical vapor deposition without a metal catalyst. ACS Nano 7:385–395
224. Chen J, Guo Y, Wen Y et al (2013) Two-stage metal-catalyst-free growth of high-quality polycrystalline graphene films on silicon nitride substrates. Adv Mater 25:992–997
225. Rümmeli MH, Bachmatiuk A, Scott A et al (2010) Direct low-temperature nanographene cvd synthesis over a dielectric insulator. ACS Nano 4:4206–4210
226. Ding X, Ding G, Xie X et al (2011) Direct growth of few layer graphene on hexagonal boron nitride by chemical vapor deposition. Carbon 49:2522–2525
227. Garcia JM, Wurstbauer U, Levy A et al (2012) Graphene growth on h-BN by molecular beam epitaxy. Solid State Commun 152:975–978
228. Tang S, Ding G, Xie X et al (2012) Nucleation and growth of single crystal graphene on hexagonal boron nitride. Carbon 50:329–331
229. Chugh S, Mehta R, Lu N et al (2015) Comparison of graphene growth on arbitrary non-catalytic substrates using low-temperature PECVD. Carbon 93:393–399
230. Kato T, Hatakeyama R (2012) Direct growth of doping-density-controlled hexagonal graphene on SiO_2 substrate by rapid-heating plasma CVD. ACS Nano 6:8508–8515
231. Li X, Magnuson CW, Venugopal A et al (2011) Large-area graphene single crystals grown by low-pressure chemical vapor deposition of methane on copper. J Am Chem Soc 133:2816–2819

232. Li X, Magnuson CW, Venugopal A et al (2010) Graphene films with large domain size by a two-step chemical vapor deposition process. Nano Lett 10:4328–4334
233. Mehdipour H, Ostrikov K (2012) Kinetics of low-pressure, low-temperature graphene growth: toward single-layer, single-crystalline structure. ACS Nano 6:10276–10286
234. Radhakrishnan G, Adams PM, Stapleton AD et al (2011) Large single-crystal monolayer graphene by decomposition of methanol. Appl Phys A 105:31–37
235. Gadipelli S, Calizo I, Ford J et al (2011) A highly practical route for large-area, single layer graphene from liquid carbon sources such as benzene and methanol. J Mater Chem 21:16057
236. Paul RK, Badhulika S, Niyogi S et al (2011) The production of oxygenated polycrystalline graphene by one-step ethanol-chemical vapor deposition. Carbon 49:3789–3795
237. Zhao P, Hou B, Chen X et al (2013) Investigation of non-segregation graphene growth on Ni via isotope-labeled alcohol catalytic chemical vapor deposition. Nanoscale 5:6530
238. Guermoune A, Chari T, Popescu F et al (2011) Chemical vapor deposition synthesis of graphene on copper with methanol, ethanol, and propanol precursors. Carbon 49:4204–4210
239. Myint M, Yan Y, Chen JG (2014) Reaction pathways of propanal and 1-propanol on Fe/Ni(111) and Cu/Ni(111) bimetallic surfaces. J Phys Chem C 118:11340–11349
240. Lisi N, Buonocore F, Dikonimos T et al (2014) Rapid and highly efficient growth of graphene on copper by chemical vapor deposition of ethanol. Thin Solid Films 571:139–144
241. Dong X, Wang P, Fang W et al (2011) Growth of large-sized graphene thin-films by liquid precursor-based chemical vapor deposition under atmospheric pressure. Carbon 49:3672–3678
242. Gao H, Liu Z, Song L et al (2012) Synthesis of S-doped graphene by liquid precursor. Nanotechnology 23:275605
243. Gullapalli H, Mohana Reddy AL, Kilpatrick S et al (2011) Graphene growth via carburization of stainless steel and application in energy storage. Small 7:1697–1700
244. Gan X, Zhou H, Zhu B et al (2012) A simple method to synthesize graphene at 633 K by dechlorination of hexachlorobenzene on Cu foils. Carbon 50:306–310
245. Dai G-P, Cooke PH, Deng S (2012) Direct growth of graphene films on TEM nickel grids using benzene as precursor. Chem Phys Lett 531:193–196
246. Wan X, Chen K, Liu D et al (2012) High-quality large-area graphene from dehydrogenated polycyclic aromatic hydrocarbons. Chem Mater 24:3906–3915
247. Kang D, Kim W-J, Lim JA, Song Y-W (2012) Direct growth and patterning of multilayer graphene onto a targeted substrate without an external carbon source. ACS Appl Mater Interfaces 4:3663–3666
248. Lee JS, Jang CW, Kim JM et al (2014) Graphene synthesis by C implantation into Cu foils. Carbon 66:267–271
249. Hackley J, Ali D, DiPasquale J et al (2009) Graphitic carbon growth on Si(111) using solid source molecular beam epitaxy. Appl Phys Lett 95:133114
250. Ji H, Hao Y, Ren Y et al (2011) Graphene growth using a solid carbon feedstock and hydrogen. ACS Nano 5:7656–7661
251. Weatherup RS, Baehtz C, Dlubak B et al (2013) Introducing carbon diffusion barriers for uniform, high-quality graphene growth from solid sources. Nano Lett 13:4624–4631
252. Shin H-J, Choi WM, Yoon S-M et al (2011) Transfer-free growth of few-layer graphene by self-assembled monolayers. Adv Mater 23:4392–4397
253. Kalita G, Sharma S, Wakita K et al (2012) Synthesis of graphene by surface wave plasma chemical vapor deposition from camphor. Phys Status Solidi 209:2510–2513
254. Kalita G, Wakita K, Umeno M (2011) Monolayer graphene from a green solid precursor. Phys E Low-dimensional Syst Nanostructures 43:1490–1493
255. Sharma S, Kalita G, Ayhan ME et al (2013) Synthesis of hexagonal graphene on polycrystalline Cu foil from solid camphor by atmospheric pressure chemical vapor deposition. J Mater Sci 48:7036–7041
256. Sharma S, Kalita G, Hirano R et al (2013) Influence of gas composition on the formation of graphene domain synthesized from camphor. Mater Lett 93:258–262
257. Sokolov AN, Yap FL, Liu N et al (2013) Direct growth of aligned graphitic nanoribbons from a DNA template by chemical vapour deposition. Nat Commun 4:2402
258. Ruan G, Sun Z, Peng Z, Tour JM (2011) Growth of graphene from food, insects, and waste. ACS Nano 5:7601–7607
259. Ray AK, Sahu RK, Rajinikanth V et al (2012) Preparation and characterization of graphene and Ni-decorated graphene using flower petals as the precursor material. Carbon 50:4123–4129
260. Hong N, Yang W, Bao C et al (2012) Facile synthesis of graphene by pyrolysis of poly(methyl methacrylate) on nickel particles in the confined microzones. Mater Res Bull 47:4082–4088
261. Kwak J, Kwon T-Y, Chu JH et al (2013) In situ observations of gas phase dynamics during graphene growth using solid-state carbon sources. Phys Chem Chem Phys 15:10446
262. Lee S, Hong J, Koo JH et al (2013) Synthesis of few-layered graphene nanoballs with copper cores using solid carbon source. ACS Appl Mater Interfaces 5:2432–2437
263. Li Z, Wu P, Wang C et al (2011) Low-temperature growth of graphene by chemical vapor deposition using solid and liquid carbon sources. ACS Nano 5:3385–3390
264. Lin T, Wang Y, Bi H et al (2012) Hydrogen flame synthesis of few-layer graphene from a solid carbon source on hexagonal boron nitride. J Mater Chem 22:2859
265. Sun Z, Yan Z, Yao J et al (2010) Growth of graphene from solid carbon sources. Nature 468:549–552
266. Tiwari RN, Ishihara M, Tiwari JN, Yoshimura M (2012) Transformation of polymer to graphene films at partially low temperature. Polym Chem 3:2712
267. Suzuki S, Takei Y, Furukawa K, Hibino H (2011) Graphene growth from a spin-coated polymer without a reactive gas. Appl Phys Express 4:065102
268. Sharma S, Kalita G, Hirano R et al (2014) Synthesis of graphene crystals from solid waste plastic by chemical vapor deposition. Carbon 72:66–73
269. Huang L, Wind SJ, O'Brien SP (2003) Controlled growth of single-walled carbon nanotubes from an ordered mesoporous silica template. Nano Lett 3:299–303
270. Homma Y, Kobayashi Y, Ogino T et al (2003) Role of transition metal catalysts in single-walled carbon nanotube growth in chemical vapor deposition. J Phys Chem B 107:12161–12164
271. Lin JH, Chen CS, Rümmeli MH et al (2011) Growth of carbon nanotubes catalyzed by defect-rich graphite surfaces. Chem Mater 23:1637–1639
272. Lin J-H, Chen C-S, Ma H-L et al (2008) Self-assembling of multi-walled carbon nanotubes on a porous carbon surface by catalyst-free chemical vapor deposition. Carbon 46:1619–1623
273. Qian W, Liu T, Wei F et al (2003) The evaluation of the gross defects of carbon nanotubes in a continuous CVD process. Carbon 41:2613–2617
274. Zhang X, Zhang J, Wang R, Liu Z (2004) Cationic surfactant directed polyaniline/CNT nanocables: synthesis, characterization, and enhanced electrical properties. Carbon 42:1455–1461
275. Zheng F, Liang Gao Y et al (2002) Carbon nanotube synthesis using mesoporous silica templates. Nano Lett 2:729–732

276. Couteau E, Hernadi K, Seo JW et al (2003) CVD synthesis of high-purity multiwalled carbon nanotubes using $CaCO_3$ catalyst support for large-scale production. Chem Phys Lett 378:9–17
277. Eres G, Puretzky AA, Geohegan DB, Cui H (2004) In situ control of the catalyst efficiency in chemical vapor deposition of vertically aligned carbon nanotubes on predeposited metal catalyst films. Appl Phys Lett 84:1759
278. Sato S, Kawabata A, Nihei M, Awano Y (2003) Growth of diameter-controlled carbon nanotubes using monodisperse nickel nanoparticles obtained with a differential mobility analyzer. Chem Phys Lett 382:361–366
279. Ibrahim I, Kalbacova J, Engemaier V et al (2015) Confirming the dual role of etchants during the enrichment of semiconducting single wall carbon nanotubes by chemical vapor deposition. Chem Mater. doi:10.1021/acs.chemmater.5b02037
280. Bachmatiuk A, Borowiak-Palen E, Rümmeli MH et al (2007) Facilitating the CVD synthesis of seamless double-walled carbon nanotubes. Nanotechnology 18:275610
281. Bachmatiuk A, Börrnert F, Grobosch M et al (2009) Investigating the graphitization mechanism of SiO_2 nanoparticles in chemical vapor deposition. ACS Nano 3:4098–4104
282. Borowiak-Palen E, Bachmatiuk A, Rümmeli MH et al (2008) Modifying CVD synthesised carbon nanotubes via the carbon feed rate. Phys E Low-dimensional Syst Nanostructures 40:2227–2230
283. Qi H, Qian C, Liu J (2006) Synthesis of high-purity few-walled carbon nanotubes from ethanol/methanol mixture. Chem Mater 18:5691–5695
284. Reina A, Hofmann M, Zhu D, Kong J (2007) Growth mechanism of long and horizontally aligned carbon nanotubes by chemical vapor deposition. J Phys Chem C 111:7292–7297
285. Liu Y, Pan C, Wang J (2004) Raman spectra of carbon nanotubes and nanofibers prepared by ethanol flames. J Mater Sci 39:1091–1094
286. Das N, Dalai A, Soltan Mohammadzadeh JS, Adjaye J (2006) The effect of feedstock and process conditions on the synthesis of high purity CNTs from aromatic hydrocarbons. Carbon 44:2236–2245
287. Shukla B, Saito T, Yumura M, Iijima S (2009) An efficient carbon precursor for gas phase growth of SWCNTs. Chem Commun 23:3422–3424
288. Tian Y, Hu Z, Yang Y et al (2004) In situ TA-MS study of the six-membered-ring-based growth of carbon nanotubes with benzene precursor. J Am Chem Soc 126:1180–1183
289. Dai H, Rinzler AG, Nikolaev P et al (1996) Single-wall nanotubes produced by metal-catalyzed disproportionation of carbon monoxide. Chem Phys Lett 260:471–475
290. Hsieh Y-P, Hofmann M, Kong J (2014) Promoter-assisted chemical vapor deposition of graphene. Carbon 67:417–423
291. Kim H, Mattevi C, Calvo MR et al (2012) Activation energy paths for graphene nucleation and growth on Cu. ACS Nano 6:3614–3623
292. Vlassiouk I, Smirnov S, Regmi M et al (2013) Graphene nucleation density on copper: fundamental role of background pressure. J Phys Chem C 117:18919–18926
293. Celebi K, Cole MT, Choi JW et al (2013) Evolutionary kinetics of graphene formation on copper. Nano Lett 13:967–974
294. Xu L, Jin Y, Wu Z et al (2013) Transformation of carbon monomers and dimers to graphene islands on Co(0001): thermodynamics and kinetics. J Phys Chem C 117:2952–2958
295. Loginova E, Bartelt NC, Feibelman PJ, McCarty KF (2008) Evidence for graphene growth by C cluster attachment. New J Phys 10:093026
296. Kim YS, Joo K, Jerng SK et al (2014) Direct integration of polycrystalline graphene into light emitting diodes by plasma-assisted metal-catalyst-free synthesis. ACS Nano 8:2230–2236
297. Kim H, Saiz E, Chhowalla M, Mattevi C (2013) Modeling of the self-limited growth in catalytic chemical vapor deposition of graphene. New J Phys 15:053012
298. Bhaviripudi S, Jia X, Dresselhaus MS, Kong J (2010) Role of kinetic factors in chemical vapor deposition synthesis of uniform large area graphene using copper catalyst. Nano Lett 10:4128–4133
299. Chen C-JCJ, Back MH, Back RA (1975) The thermal decomposition of methane. I. kinetics of the primary decomposition to $C_2H_6 + H_2$; rate constant for the homogeneous unimolecular dissociation of methane and its pressure dependence. Can J Chem 53:3580–3590
300. Alstrup I, Chorkendorff I, Ullmann S (1992) The interaction of CH_4 at high temperatures with clean and oxygen precovered Cu(100). Surf Sci 264:95–102
301. Zhang Y, Zhang L, Kim P et al (2012) Vapor trapping growth of single-crystalline graphene flowers: synthesis, morphology, and electronic properties. Nano Lett 12:2810–2816
302. Kidambi PR, Bayer BC, Blume R et al (2013) Observing graphene grow: catalyst-graphene interactions during scalable graphene growth on polycrystalline copper. Nano Lett 13:4769–4778
303. Wang Z-J, Weinberg G, Zhang Q et al (2015) Direct observation of graphene growth and associated copper substrate dynamics by in situ scanning electron microscopy. ACS Nano 9:1506–1519
304. N'Diaye AT, van Gastel R, Martínez-Galera AJ et al (2009) In situ observation of stress relaxation in epitaxial graphene. New J Phys 11:113056
305. Nie S, Walter AL, Bartelt NC et al (2011) Growth from below: graphene bilayers on Ir(111). ACS Nano 5:2298–2306
306. Weatherup RS, Bayer BC, Blume R et al (2011) In situ characterization of alloy catalysts for low-temperature graphene growth. Nano Lett 11:4154–4160
307. Xing S, Wu W, Wang Y et al (2013) Kinetic study of graphene growth: temperature perspective on growth rate and film thickness by chemical vapor deposition. Chem Phys Lett 580:62–66
308. Colombo L, Li X, Han B et al (2010) Growth kinetics and defects of CVD graphene on Cu. ECS Trans 28(5):109–114
309. Han Z, Kimouche A, Kalita D et al (2014) Homogeneous optical and electronic properties of graphene due to the suppression of multilayer patches during CVD on copper foils. Adv Funct Mater 24:964–970
310. Fang W, Hsu A, Shin YC et al (2015) Application of tungsten as a carbon sink for synthesis of large-domain uniform monolayer graphene free of bilayers/multilayers. Nanoscale 7:4929–4934
311. Pan Z, Liu N, Fu L, Liu Z (2011) Wrinkle engineering: a new approach to massive graphene nanoribbon arrays. J Am Chem Soc 133:17578–17581
312. Fang W, Hsu AL, Caudillo R et al (2013) Rapid identification of stacking orientation in isotopically labeled chemical-vapor grown bilayer graphene by raman spectroscopy. Nano Lett 13:1541–1548
313. Li Q, Chou H, Zhong J-H et al (2013) Growth of adlayer graphene on Cu studied by carbon isotope labeling. Nano Lett 13:486–490
314. Nie S, Wu W, Xing S et al (2012) Growth from below: bilayer graphene on copper by chemical vapor deposition. New J Phys 14:093028
315. Kalbac M, Frank O, Kavan L (2012) The control of graphene double-layer formation in copper-catalyzed chemical vapor deposition. Carbon 50:3682–3687
316. Robertson AW, Warner JH (2011) Hexagonal Single crystal domains of few-layer graphene on copper foils. Nano Lett 11:1182–1189
317. Geng D, Wu B, Guo Y et al (2012) Uniform hexagonal graphene flakes and films grown on liquid copper surface. Proc Natl Acad Sci 109:7992–7996

318. Wang J, Zeng M, Tan L et al (2013) High-mobility graphene on liquid p-block elements by ultra-low-loss CVD growth. Sci Rep 3:2670
319. Wu Y, Hao Y, Jeong HY et al (2013) Crystal structure evolution of individual graphene islands during CVD growth on copper foil. Adv Mater 25:6744–6751
320. Murdock AT, Koos A, Ben Britton T et al (2013) Controlling the orientation, edge geometry, and thickness of chemical vapor deposition graphene. ACS Nano 7:1351–1359
321. Hayashi K, Sato S, Ikeda M et al (2012) Selective graphene formation on copper twin crystals. J Am Chem Soc 134:12492–12498
322. Wood JD, Schmucker SW, Lyons AS et al (2011) Effects of polycrystalline Cu substrate on graphene growth by chemical vapor deposition. Nano Lett 11:4547–4554
323. Dai G-P, Wu MH, Taylor DK, Vinodgopal K (2013) Square-shaped, single-crystal, monolayer graphene domains by low-pressure chemical vapor deposition. Mater Res Lett 1:67–76
324. Son IH, Song HJ, Kwon S et al (2014) CO_2 enhanced chemical vapor deposition growth of few-layer graphene over NiOx. ACS Nano 8:9224–9232
325. Natesan K, Kassner TF (1973) Thermodynamics of carbon in nickel, iron-nickel and iron-chromium-nickel alloys. Metall Trans 4:2557–2566
326. Delamoreanu A, Rabot C, Vallee C, Zenasni A (2014) Wafer scale catalytic growth of graphene on nickel by solid carbon source. Carbon 66:48–56
327. Lahiri J, Miller T, Adamska L et al (2011) Graphene growth on Ni(111) by transformation of a surface carbide. Nano Lett 11:518–522
328. Thiele S, Reina A, Healey P et al (2010) Engineering polycrystalline Ni films to improve thickness uniformity of the chemical-vapor-deposition-grown graphene films. Nanotechnology 21:015601
329. Kim H, Song I, Park C et al (2013) Copper-vapor-assisted chemical vapor deposition for high-quality and metal-free single-layer graphene on amorphous SiO2 substrate. ACS Nano 7:6575–6582
330. Zhang L, Shi Z, Liu D et al (2012) Vapour-phase graphene epitaxy at low temperatures. Nano Res 5:258–264
331. Wei D, Lu Y, Han C et al (2013) Critical crystal growth of graphene on dielectric substrates at low temperature for electronic devices. Angew Chemie Int Ed 52:14121–14126
332. Li X, Zhu Y, Cai W et al (2009) Transfer of large-area graphene films for high-performance transparent conductive electrodes. Nano Lett 9:4359–4363
333. Suk JW, Kitt A, Magnuson CW et al (2011) Transfer of CVD-grown monolayer graphene onto arbitrary substrates. ACS Nano 5:6916–6924
334. O'Hern SC, Stewart CA, Boutilier MSH et al (2012) Selective molecular transport through intrinsic defects in a single layer of CVD graphene. ACS Nano 6:10130–10138
335. Pirkle A, Chan J, Venugopal A et al (2011) The effect of chemical residues on the physical and electrical properties of chemical vapor deposited graphene transferred to SiO_2. Appl Phys Lett 99:122108
336. Lin Y-C, Jin C, Lee J-C et al (2011) Clean transfer of graphene for isolation and suspension. ACS Nano 5:2362–2368
337. Gorantla S, Bachmatiuk A, Hwang J et al (2014) A universal transfer route for graphene. Nanoscale 6:889–896
338. Gao L, Ren W, Xu H et al (2012) Repeated growth and bubbling transfer of graphene with millimetre-size single-crystal grains using platinum. Nat Commun 3:699
339. Wang Y, Zheng Y, Xu X et al (2011) Electrochemical delamination of CVD-grown graphene film: toward the recyclable use of copper catalyst. ACS Nano 5:9927–9933
340. Lin W-HH, Chen T-HH, Chang J-KK et al (2014) A direct and polymer-free method for transferring graphene grown by chemical vapor deposition to any substrate. ACS Nano 8:1784–1791
341. Na SR, Suk JW, Tao L et al (2015) Selective mechanical transfer of graphene from seed copper foil using rate effects. ACS Nano 9:1325–1335
342. Lee WH, Suk JW, Lee J et al (2012) Simultaneous transfer and doping of CVD-grown graphene by fluoropolymer for transparent conductive films on plastic. ACS Nano 6:1284–1290
343. Gao L, Ni G-X, Liu Y et al (2013) Face-to-face transfer of wafer-scale graphene films. Nature 505:190–194
344. Ding L, Tselev A, Wang J et al (2009) Selective growth of well-aligned semiconducting single-walled carbon nanotubes. Nano Lett 9:800–805
345. Williams KR, Gupta K, Wasilik M (2003) Etch rates for micromachining processing-part II. J Microelectromechanical Syst 12(6):761–778
346. Rümmeli M, Bachmatiuk A, Börrnert F et al (2011) Synthesis of carbon nanotubes with and without catalyst particles. Nanoscale Res Lett 6:303
347. Ding L, Zhou W, McNicholas TP et al (2009) Direct observation of the strong interaction between carbon nanotubes and quartz substrate. Nano Res 2:903–910
348. Ibrahim I, Bachmatiuk A, Börrnert F et al (2011) Optimizing substrate surface and catalyst conditions for high yield chemical vapor deposition grown epitaxially aligned single-walled carbon nanotubes. Carbon 49:5029–5037
349. Ci L, Rao Z, Zhou Z et al (2002) Double wall carbon nanotubes promoted by sulfur in a floating iron catalyst CVD system. Chem Phys Lett 359:63–67
350. Loffler M, Rummeli MH, Kramberger C et al (2008) On the formation of single-walled carbon nanotubes in pulsed-laser-assisted chemical vapor deposition. Chem Mater 20:128–134
351. Hata K, Futaba D, Mizuno K et al (2004) Water-assisted highly efficient synthesis of impurity-free single-walled carbon nanotubes. Science 306:1362–1364
352. Yamada T, Namai T, Hata K et al (2006) Size-selective growth of double-walled carbon nanotube forests from engineered iron catalysts. Nat Nanotechnol 1:131–136
353. Huang S, Cai X, Liu J (2003) Growth of millimeter-long and horizontally aligned single-walled carbon nanotubes on flat substrates. J Am Chem Soc 125:5636–5637
354. Ibrahim I, Bachmatiuk A, Grimm D et al (2012) Understanding high-yield catalyst-free growth of horizontally aligned single-walled carbon nanotubes nucleated by activated C60 species. ACS Nano 6:10825–10834
355. Ibrahim I, Bachmatiuk A, Warner JH et al (2012) CVD-grown horizontally aligned single-walled carbon nanotubes: synthesis routes and growth mechanisms. Small 8:1973–1992
356. Joselevich E, Lieber CM (2002) Vectorial growth of metallic and semiconducting single-wall carbon nanotubes. Nano Lett 2:1137–1141
357. Liu B, Ren W, Gao L et al (2009) Metal-catalyst-free growth of single-walled carbon nanotubes. J Am Chem Soc 131:2082–2083
358. Maruyama S, Kojima R, Miyauchi Y et al (2002) Low-temperature synthesis of high-purity single-walled carbon nanotubes from alcohol. Chem Phys Lett 360:229–234
359. Takagi D, Kobayashi Y, Homma Y (2009) Carbon nanotube growth from diamond. J Am Chem Soc 131:6922–6923
360. Liu J, Wang C, Tu X et al (2012) Chirality-controlled synthesis of single-wall carbon nanotubes using vapour-phase epitaxy. Nat Commun 3:1199
361. Yao Y, Feng C, Zhang J, Liu Z (2009) Cloning of single-walled carbon nanotubes via open-end growth mechanism. Nano Lett 9:1673–1677

362. Cheng H-C, Lin K-C, Tai H-C et al (2007) Growth and field emission characteristics of carbon nanotubes using Co/Cr/Al multilayer catalyst. Jpn J Appl Phys 46:4359–4363
363. Chhowalla M, Teo KBK, Ducati C et al (2001) Growth process conditions of vertically aligned carbon nanotubes using plasma enhanced chemical vapor deposition. J Appl Phys 90:5308
364. Ducati C, Alexandrou I, Chhowalla M et al (2002) Temperature selective growth of carbon nanotubes by chemical vapor deposition. J Appl Phys 92:3299–3303
365. Kim K-EK-J, Kim K-EK-J, Jung WS et al (2005) Investigation on the temperature-dependent growth rate of carbon nanotubes using chemical vapor deposition of ferrocene and acetylene. Chem Phys Lett 401:459–464
366. Picher M, Navas H, Arenal R et al (2012) Influence of the growth conditions on the defect density of single-walled carbon nanotubes. Carbon 50:2407–2416
367. Hofmann S, Ducati C, Kleinsorge B, Robertson J (2003) Direct growth of aligned carbon nanotube field emitter arrays onto plastic substrates. Appl Phys Lett 83:4661–4663
368. Ding F, Bolton K, Rosén A (2004) Nucleation and growth of single-walled carbon nanotubes: a molecular dynamics study. J Phys Chem B. 108(45):17369–17377
369. Kukovitsky EF, L'vov SG, Sainov NA (2000) VLS-growth of carbon nanotubes from the vapor. Chem Phys Lett 317:65–70
370. Kukovitsky EF, L'vov SG, Sainov NA et al (2002) Correlation between metal catalyst particle size and carbon nanotube growth. Chem Phys Lett 355:497–503
371. Shibuta Y, Suzuki T (2010) Melting and solidification point of fcc-metal nanoparticles with respect to particle size: a molecular dynamics study. Chem Phys Lett 498:323–327
372. Harutyunyan AR, Tokune T, Mora E (2005) Liquid as a required catalyst phase for carbon single-walled nanotube growth. Appl Phys Lett 87:051919
373. Hofmann S, Csányi G, Ferrari AC et al (2005) Surface diffusion: the low activation energy path for nanotube growth. Phys Rev Lett 95:036101
374. Klinke C, Bonard JM, Kern K (2005) Thermodynamic calculations on the catalytic growth of multiwall carbon nanotubes. Phys Rev B 71:035403
375. Barreiro A, Kramberger C, Rümmeli MH et al (2007) Control of the single-wall carbon nanotube mean diameter in sulphur promoted aerosol-assisted chemical vapour deposition. Carbon 45:55–61
376. Cheung CL, Kurtz A, Park H, Lieber CM (2002) Diameter-controlled synthesis of carbon nanotubes. J Phys Chem B 106:2429–2433
377. Schäffel F, Kramberger C, Rümmeli MH et al (2007) Nano-engineered catalyst particles as a key for tailor-made carbon nanotubes. Chem Mater 19:5006–5009
378. Thurakitseree T, Kramberger C, Zhao P et al (2012) Diameter-controlled and nitrogen-doped vertically aligned single-walled carbon nanotubes. Carbon 50:2635–2640
379. Marchand M, Journet C, Guillot D et al (2009) Growing a carbon nanotube atom by atom: "and yet it does turn". Nano Lett 9:2961–2966
380. Neyts EC, Van Duin ACT, Bogaerts A (2011) Changing chirality during single-walled carbon nanotube growth: a reactive molecular dynamics/monte carlo study. J Am Chem Soc 133:17225–17231
381. Wang Q, Ng MF, Yang SW et al (2010) The mechanism of single-walled carbon nanotube growth and chirality selection induced by carbon atom and dimer addition. ACS Nano 4:939–946
382. Hart AJ, Van Laake L, Slocum AH (2007) Desktop growth of carbon-nanotube monoliths with in situ optical imaging. Small 3:772–777
383. Geohegan DB, Puretzky AA, Ivanov IN et al (2003) In situ growth rate measurements and length control during chemical vapor deposition of vertically aligned multiwall carbon nanotubes. Appl Phys Lett 83:1851–1853
384. Puretzky AA, Geohegan DB, Jesse S et al (2005) In situ measurements and modeling of carbon nanotube array growth kinetics during chemical vapor deposition. Appl Phys A 81:223–240
385. Einarsson E, Murakami Y, Kadowaki M, Maruyama S (2008) Growth dynamics of vertically aligned single-walled carbon nanotubes from in situ measurements. Carbon 46:923–930
386. Chiashi S, Murakami Y, Miyauchi Y, Maruyama S (2004) Cold wall CVD generation of single-walled carbon nanotubes and in situ Raman scattering measurements of the growth stage. Chem Phys Lett 386:89–94
387. Picher M, Anglaret E, Arenal R, Jourdain V (2009) Self-deactivation of single-walled carbon nanotube growth studied by in situ Raman measurements. Nano Lett 9:542–547
388. Rao R, Liptak D, Cherukuri T et al (2012) In situ evidence for chirality-dependent growth rates of individual carbon nanotubes. Nat Mater 11:213–216
389. Reinhold-López K, Braeuer A, Romann B et al (2014) Simultaneous in situ Raman monitoring of the solid and gas phases during the formation and growth of carbon nanostructures inside a cold wall CCVD reactor. Carbon 78:164–180
390. Nishimura K, Okazaki N, Pan L, Nakayama Y (2004) In situ study of iron catalysts for carbon nanotube growth using X-ray diffraction analysis. Jpn J Appl Phys 43:L471–L474
391. Mattevi C, Wirth CT, Hofmann S et al (2008) In-situ X-ray photoelectron spectroscopy study of catalyst-support interactions and growth of carbon nanotube forests. J Phys Chem C 112:12207–12213
392. Lin M, Ying Tan JP, Boothroyd C et al (2006) Direct observation of single-walled carbon nanotube growth at the atomistic scale. Nano Lett 6:449–452
393. Yoshida H, Takeda S, Uchiyama T et al (2008) Atomic-scale in-situ observation of carbon nanotube growth from solid state iron carbide nanoparticles. Nano Lett 8:2082–2086
394. Zhang L, Hou PX, Li S et al (2014) In situ TEM observations on the sulfur-assisted catalytic growth of single-wall carbon nanotubes. J Phys Chem Lett 5:1427–1432
395. Futaba DN, Hata K, Yamada T et al (2005) Kinetics of water-assisted single-walled carbon nanotube synthesis revealed by a time-evolution analysis. Phys Rev Lett 95:056104
396. Helveg S, López-Cartes C, Sehested J et al (2004) Atomic-scale imaging of carbon nanofibre growth. Nature 427:426–429
397. Stadermann M, Sherlock SP, In J-B et al (2009) Mechanism and kinetics of growth termination in controlled chemical vapor deposition growth of multiwall carbon nanotube arrays. Nano Lett 9:738–744
398. Yamada T, Maigne A, Yudasaka M et al (2008) Revealing the secret of water-assisted carbon nanotube synthesis by microscopic observation of the interaction of water on the catalysts. Nano Lett 8:4288–4292
399. Nishino H, Yasuda S, Namai T et al (2007) Water-assisted highly efficient synthesis of single-walled carbon nanotubes forests from colloidal nanoparticle catalysts. J Phys Chem C 111:17961–17965
400. Pint CL, Pheasant ST, Parra-Vasquez ANG et al (2009) Investigation of optimal parameters for oxide-assisted growth of vertically aligned single-walled carbon nanotubes. J Phys Chem C 113:4125–4133
401. Reilly PTA, Whitten WB (2006) The role of free radical condensates in the production of carbon nanotubes during the hydrocarbon CVD process. Carbon 44:1653–1660

402. Schünemann C, Schäffel F, Bachmatiuk A et al (2011) Catalyst poisoning by amorphous carbon during carbon nanotube growth: fact or fiction? ACS Nano 5:8928–8934
403. Xiang R, Yang Z, Zhang Q et al (2008) Growth deceleration of vertically aligned carbon nanotube arrays: catalyst deactivation or feedstock diffusion controlled? J Phys Chem C 112: 4892–4896
404. Bedewy M, Meshot ER, Guo H et al (2009) Collective mechanism for the evolution and self-termination of vertically aligned carbon nanotube growth. J Phys Chem C 113:20576–20582
405. Bower C, Zhou O, Zhu W et al (2000) Nucleation and growth of carbon nanotubes by microwave plasma chemical vapor deposition. Appl Phys Lett 77:2767–2769
406. Li J, Papadopoulos C, Xu JM, Moskovits M (1999) Highly-ordered carbon nanotube arrays for electronics applications. Appl Phys Lett 75:367–369
407. Kumar M, Ando Y (2010) Chemical vapor deposition of carbon nanotubes: a review on growth mechanism and mass production. J Nanosci Nanotechnol 10:3739–3758
408. Rodriguez NM (1993) A review of catalytically grown carbon nanofibers. J Mater Res 8:3233–3250
409. Tibbetts GG (1984) Why are carbon filaments tubular? J Cryst Growth 66:632–638
410. Ding F, Bolton K, Rosén A (2006) Molecular dynamics study of SWNT growth on catalyst particles without temperature gradients. Comput Mater Sci 35:243–246
411. Bolton K, Ding F, Rosén A (2006) Atomistic simulations of catalyzed carbon nanotube growth. J Nanosci Nanotechnol 6:1211–1224
412. Kitiyanan B, Alvarez WE, Harwell JH, Resasco DE (2000) Controlled production of single-wall carbon nanotubes by catalytic decomposition of CO on bimetallic Co–Mo catalysts. Chem Phys Lett 317:497–503
413. Li Y, Liu J, Wang Y, Wang ZL (2001) Preparation of monodispersed Fe–Mo nanoparticles as the catalyst for CVD synthesis of carbon nanotubes. Chem Mater 13:1008–1014
414. Thurakitseree T, Einarsson E, Xiang R et al (2012) Diameter controlled chemical vapor deposition synthesis of single-walled carbon nanotubes. J Nanosci Nanotechnol 12:370–376
415. Ayala P, Grüneis A, Gemming T et al (2007) Tailoring N-doped single and double wall carbon nanotubes from a nondiluted carbon/nitrogen feedstock. J Phys Chem C 111:2879–2884
416. Cassell MA, Raymakers AJ, Kong J et al (1999) Large scale CVD synthesis of single-walled carbon nanotubes. J Phys Chem B 103:6484–6492
417. Liu B, Ren W, Li S et al (2012) High temperature selective growth of single-walled carbon nanotubes with a narrow chirality distribution from a CoPt bimetallic catalyst. Chem Commun 48:2409
418. Yang F, Wang X, Zhang D et al (2014) Chirality-specific growth of single-walled carbon nanotubes on solid alloy catalysts. Nature 510:522–524
419. Wang H, Wei L, Ren F et al (2013) Chiral-selective $CoSo_4/SiO_2$ catalyst for (9,8) single-walled carbon nanotube growth. ACS Nano 7:614–626
420. Wang H, Wang B, Quek XY et al (2010) Selective synthesis of (9,8) single walled carbon nanotubes on cobalt incorporated TUD-1 catalysts. J Am Chem Soc 132:16747–16749
421. He M, Jiang H, Liu B et al (2013) Chiral-selective growth of single-walled carbon nanotubes on lattice-mismatched epitaxial cobalt nanoparticles. Sci Rep 3:1460
422. Ding F, Harutyunyan AR, Yakobson BI (2009) Dislocation theory of chirality-controlled nanotube growth. Proc Natl Acad Sci USA 106:2506–2509
423. Ibrahim I, Zhang Y, Popov A et al (2013) Growth of all-carbon horizontally aligned single-walled carbon nanotubes nucleated from fullerene-based structures. Nanoscale Res Lett 8:265
424. Yu X, Zhang J, Choi W et al (2010) Cap formation engineering: from opened C60 to single-walled carbon nanotubes. Nano Lett 10:3343–3349
425. Liu Y, Xu M, Zhu X et al (2014) Synthesis of carbon nanotubes on graphene quantum dot surface by catalyst free chemical vapor deposition. Carbon 68:399–405
426. Takagi D, Hibino H, Suzuki S et al (2007) Carbon nanotube growth from semiconductor nanoparticles. Nano Lett 7:2272–2275
427. Scott A, Dianat A, Börrnert F et al (2011) The catalytic potential of high-κ dielectrics for graphene formation. Appl Phys Lett 98:073110
428. Huang S, Cai Q, Chen J et al (2009) Metal-catalyst-free growth of single-walled carbon nanotubes on substrates. J Am Chem Soc 131:2094–2095
429. Liu B, Tang DM, Sun C et al (2011) Importance of oxygen in the metal-free catalytic growth of single-walled carbon nanotubes from SiOx by a vapor-solid-solid mechanism. J Am Chem Soc 133:197–199
430. Kang L, Hu Y, Liu L et al (2015) Growth of close-packed semiconducting single-walled carbon nanotube arrays using oxygen-deficient TiO_2 nanoparticles as catalysts. Nano Lett 15:403–409
431. Steiner SA, Baumann TF, Bayer BC et al (2009) Nanoscale zirconia as a nonmetallic catalyst for graphitization of carbon and growth of single- and multiwall carbon nanotubes. J Am Chem Soc 131:12144–12154
432. Kudo A, Steiner SA, Bayer BC et al (2014) CVD growth of carbon nanostructures from zirconia: mechanisms and a method for enhancing yield. J Am Chem Soc 136:17808–17817
433. Ning G, Xu C, Zhu X et al (2013) MgO-catalyzed growth of N-doped wrinkled carbon nanotubes. Carbon 56:38–44
434. Gao F, Zhang L, Huang S (2010) Zinc oxide catalyzed growth of single-walled carbon nanotubes. Appl Surf Sci 256:2323–2326
435. Lin J-H, Chen C-S, Rümmeli MH, Zeng Z-Y (2010) Self-assembly formation of multi-walled carbon nanotubes on gold surfaces. Nanoscale 2:2835–2840
436. Liu BL, Ren WC, Gao LB et al (2008) Manganese-catalyzed surface growth of single-walled carbon nanotubes with high efficiency. J Phys Chem C 112:19231–19235
437. Yuan D, Ding L, Chu H et al (2008) Horizontally aligned single-walled carbon nanotube on quartz from a large variety of metal catalysts. Nano Lett 8:2576–2579
438. Takagi D, Homma Y, Hibino H et al (2006) Single-walled carbon nanotube growth from highly activated metal nanoparticles. Nano Lett 6:2642–2645
439. Zhou W, Han Z, Wang J et al (2006) Copper catalyzing growth of single-walled carbon nanotubes on substrates. Nano Lett 6:2987–2990
440. Mizutani Y, Fukuoka N, Naritsuka S et al (2012) Single-walled carbon nanotube synthesis on SiO2/Si substrates at very low pressures by the alcohol gas source method using a Pt catalyst. Diam Relat Mater 26:78–82
441. Ritschel M, Leonhardt A, Elefant D et al (2007) Rhenium-catalyzed growth carbon nanotubes. J Phys Chem C 111: 8414–8417
442. Xu X, Yang C, Yang Z et al (2014) Carbon nanotube growth from alkali metal salt nanoparticles. Carbon 80:490–495